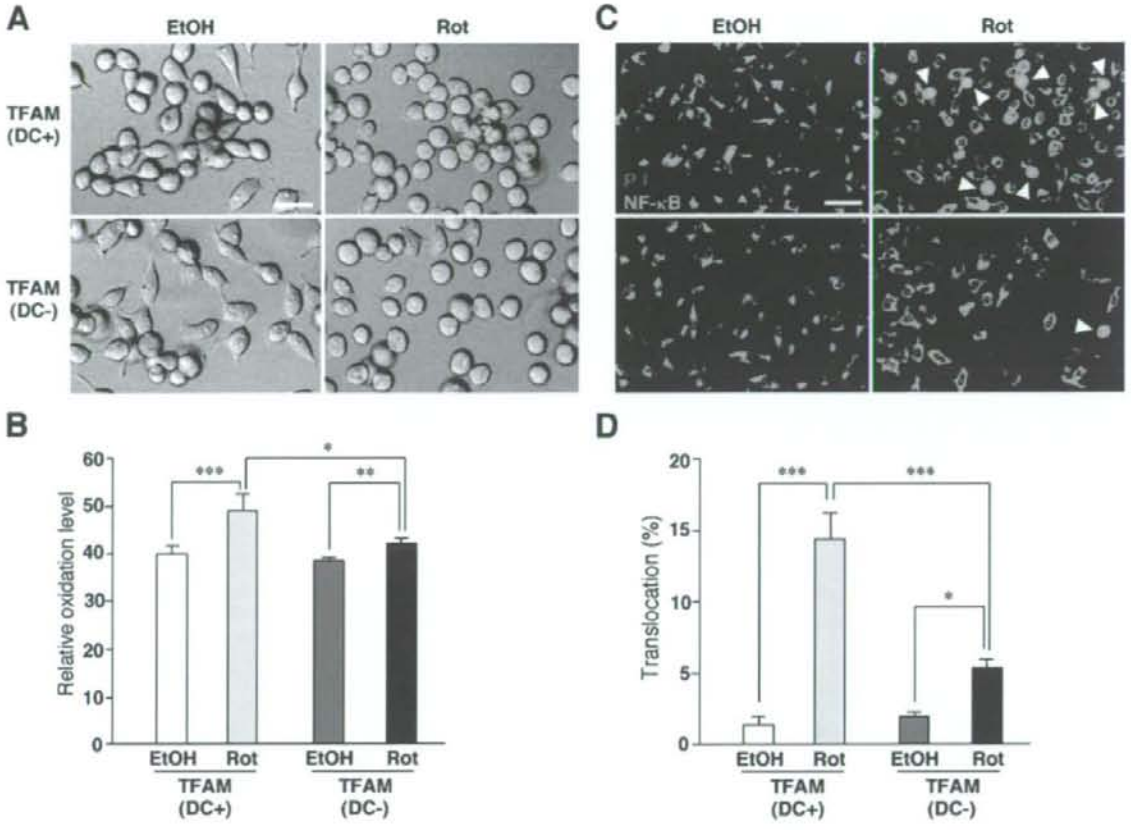

Figure 2. Effects of an overexpression of TFAM by the tetracycline-off system on rotenone-induced intracellular ROS generation and NF-κB nuclear translocation in HeLa cells. ***A***, CLMS images of rotenone-induced intracellular ROS generation measured using a ROS-sensitive dye (green), DHE, in HeLa cells cultured with or without DC. Scale bar, 20 μm. ***B***, The mean DHE oxidation levels in HeLa cells cultured with or without DC after treatment with EtOH or rotenone. Each column and bar represent the mean ± SEM of six experiments. The asterisks indicate a significant difference between two groups (*$p < 0.05$; **$p < 0.01$; ***$p < 0.001$). ***C***, NF-κB (green) and propidium iodide (PI)-stained nuclei (red) in HeLa cells cultured with or without DC after the treatment with EtOH or rotenone. The arrowheads show HeLa cells with the nuclear translocated NF-κB. Scale bar, 50 μm. ***D***, The mean percentage of the NF-κB nuclear translocation in HeLa cells cultured with or without DC after the treatment with EtOH or rotenone. Each column and bar represent the mean ± SEM of nine experiments. The asterisks indicate significant differences between two groups (*$p < 0.05$; ***$p < 0.001$). Rot, Rotenone.

Mitochondrial enzyme activities. Twenty male C57BL/6 mice (WT and TG) of the following age groups: young (2 months of age; WT, $n = 5$; TG, $n = 5$) and aged (24 months of age; WT, $n = 5$; TG, $n = 5$) were used to measure the mitochondrial enzyme activities. The specific activity of mitochondrial complex enzymes, including complexes I, II, III, and IV, was measured in mitochondria isolated from whole brains of each group as described previously (Ide et al., 1999). The specific activity of rotenone-sensitive NADH-ubiquinone oxidoreductase (complex I) was measured by reduction of the ubiquinone analog decylubiquinone. For the activity of succinate ubiquinone oxidoreductase (complex II), the reduction of 2,6-dichlorophenolindophenol when coupled to complex II-catalyzed reduction of decylubiquinone was measured. For the specific activity of ubiquinol/cytochrome *c* oxidoreductase (complex III), the reduction of cytochrome *c* catalyzed by complex III in the presence of reduced decylubiquinone was monitored. The specific activity of cytochrome *c* oxidase (complex IV) was measured by following the oxidation of reduced cytochrome *c*, which was prepared in the presence of dithionite. All enzymatic activities were expressed as nanomoles per minute per milligram of protein.

Immunohistochemistry. Twenty-four male C57BL/6 mice (WT and TG) of the following age groups: young (2–4 months of age; WT, $n = 6$; TG, $n = 6$) and aged (20–24 months of age; WT, $n = 6$; TG, $n = 6$) were used for the immunohistochemical analyses. WT and TG mice of both young and aged groups were anesthetized with sodium pentobarbital (40 mg/kg, i.p.) and killed by intracardiac perfusion with isotonic saline followed by PBS, pH 7.4. After perfusion, the brain was removed and further fixed by immersion in 4% paraformaldehyde overnight at 4°C, and then immersed in 30% sucrose for 24 h at 4°C. Floating coronal sections (10 μm thick) of the hippocampus were prepared by a cryostat and stained with anti-human TFAM, anti-8-oxo-deoxyguanosine (8-oxo-dG) (NOF Corporation), anti-4-hydroxy-2-nonenal (HNE) (Alpha Diagnostic), and anti-interleukin-1β (IL-1β) (Santa Cruz Biotechnology) for 3 d at 4°C. To detect any oxidative damage in the mitochondrial DNA rather than in the nuclear DNA, the sections were directly treated with anti-8-oxo-dG antibody without treatment of HCl as described previously (Kajitani et al., 2006). After washing with PBS, the sections were stained using the avidin–biotin–peroxidase complex method (Vector Laboratories). After washing with PBS, the sections were reacted with 0.015% 3′,3-diaminobenzidine/0.4% $(NH_4)_2Ni(SO_4)_2$/0.09% H_2O_2/0.1 mol/l Tris-buffered saline for 5–10 min. The sections were rinsed thoroughly with PBS, mounted, and coverslipped. As negative controls, the sections were incubated with nonimmune rabbit IgG or mouse IgG instead of the first antibody and processed in the same manner as described above.

For double fluorescent staining, the floating sections were stained with the following combinations of the first antibodies for 48 h at 4°C: anti-

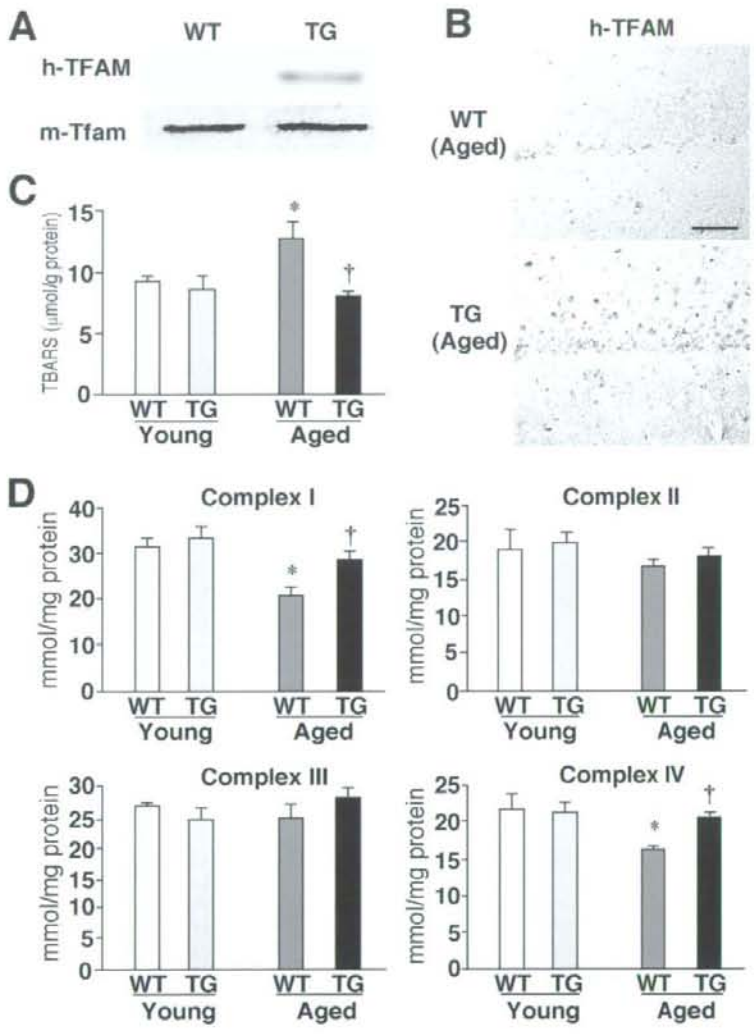

Figure 3. The effects of TFAM overexpression on age-dependent increased oxidative stress in the brain. ***A***, Expression of TFAM in the brain. Immunoblotting was performed using specific antibodies against human TFAM (h-TFAM) and mouse Tfam (m-Tfam) in soluble brain extracts prepared from the young WT and TG mice. ***B***, Immunohistochemical staining for H-TFAM in the CA1 hippocampal subfield of aged WT and TG mice. Scale bar, 50 μm. ***C***, The mean lipid peroxidation levels measured using a biochemical assay for TBARS in the brain tissues prepared from the WT and TG mice of both age groups. Each column and bar represent the mean ± SEM of five experiments. An asterisk indicates a significant difference versus the young WT mice ($^*p < 0.05$). A dagger indicates a significant difference versus the aged WT mice ($^\dagger p < 0.05$). ***D***, The mean activity of mitochondrial respiratory enzymes, complexes I to IV, in brain tissues prepared from the WT and TG mice of both age groups. Each column and bar represent the mean ± SEM of five experiments. The asterisks indicate significant differences versus the young WT mice ($^*p < 0.05$). The daggers indicate significant differences versus the aged WT mice ($^\dagger p < 0.05$).

8-oxo-dG and anti-Iba1 IgGs (Wako Pure Chemicals Industries); anti-8-oxo-dG and anti-GFAP IgGs (Sigma-Aldrich); anti-8-oxo-dG and anti-MAP2 IgGs (Millipore Bioscience Research Reagents); anti-HNE IgG and F4/80 (Serotec); anti-HNE and anti-GFAP IgGs; anti-HNE and anti-NeuN IgGs (Millipore Bioscience Research Reagents); anti-IL-1β and anti-Iba1 IgGs; anti-IL-1β and anti-GFAP IgGs; anti-IL-1β and anti-NeuN IgGs; 8-oxo-dG and anti-cytochrome *b* (Cyt *b*) IgGs (Kanki et al., 2004b). After washing with PBS, the sections were incubated with a mixture of 0.5% Alexa 488 anti-mouse IgG and Cy3 anti-rabbit IgG, 0.5% Alexa 488 anti-rabbit IgG and Cy3 anti-mouse IgG (GE Healthcare) for 2 h at room temperature. Some sections immunostained using anti-8-oxo-dG and anti-HNE IgGs were stained with an RNA/DNA marker, YOYO-1 (Invitrogen). After several washes with PBS, the sections were mounted in the antifading medium Vectashield (Vector Laboratories) and examined with a CLSM (LSM510MET; Carl Zeiss). To quantitatively assess the immunofluorescence intensity of IL-1β in microglia, the immunofluorescence intensity of IL-1β within Iba1-positive cells was measured as the average pixel intensity. The immunofluorescence intensity of 8-oxo-dG within Cyt *b*-positive mitochondria was also measured as the average pixel intensity.

Behavioral tests. Twenty-four male C57BL/6 mice (WT and TG) of the following age groups: young (2 months of age; WT, $n = 6$; TG, $n = 6$) and aged (24 months of age; WT, $n = 6$; TG, $n = 6$) were used in the following behavioral tests.

For the cylinder test, the modified cylinder test was used to monitor locomotor activity in a novel environment (Tillerson et al., 2002). In short, each animal was placed in a glass cylinder (diameter, 10 cm; height, 14 cm) and was videotaped for 6 min. The mice responded to the novel environment by standing on their hindlimbs and leaning on the walls of the cylinder with their forelimbs. The number of supporting paw placements performed independently with the left and the right paws were counted for the first 3 min. The forelimb use score was described by expressing the total number of wall contacts performed with both forelimbs.

For the measurement of locomotor activities, mice were removed from their home cages and placed in a novel home cage (clean and without bedding), which provided a floor area of 28 × 18 cm, and then the locomotor activity of mice of each genotype and each different age group was scored for 3 min. The novel home cage was divided into six identical rectangles and a trained observer determined the incidence of line crossing.

For the rotarod test, an automated single lane rotarod treadmill (Muromachi; 3 cm diameter drums with grooves to improve the grip) that could be set at either a fixed speed or an accelerating speed was used. For the fixed speed rotarod protocol, all mice were pretrained on the rotarod apparatus in order for them to reach a stable performance as described by Iancu et al. (2005). The training consisted of three sessions on 2 consecutive days, whereby each session included three separate test trials, each lasting 120 s. The mice were trained at 5, 10, and 15 rpm. On day 1, mice were trained at 5 rpm. On day 2, mice were trained once in the morning at 10 rpm and once again in the afternoon at 15 rpm. The final test (three sessions, each lasting 180 s) was performed on the third day at 15 rpm. For each trial, the mouse was gently placed on the stopped rod, with its body axis perpendicular to the rotation axis and the head oriented to the same direction of rotation, so that the animal had to turn their position against the direction of rotation and progress forward to avoid a fall from the rod after the rod started to rotate. Between trials, the mice were given at least 10 min of rest to reduce stress and fatigue. The length of time that each animal was able to stay on the rod was recorded as the latency to fall, and it was registered automatically by a trip switch under the floor of the rotating drum.

For the radial maze test, an apparatus was created as described previ-

ously (Morgan et al., 2000). The radial-arm water maze consisted of a circular pool measuring 1 m in diameter with six arms 19 cm wide that radiated out from an open central area, with a submerged escape platform located at the end of one of the arms. Spatial cues including a light were present on the wall of the testing room. The escape platform was placed in a different arm each day, forcing the mouse to use working memory to solve the task. On each trial, the mouse was started in one arm and allowed to swim for up to 1 min until finding the platform. The number of errors until the mouse reached the platform was recorded. After the fourth trial, the mouse was placed in a cage for 30 min and then returned to the maze and administered the fifth trial to assess memory retention. The error score was determined by the average score obtained from testing conducted during a 2 d period after training for 7 d.

Systemic lipopolysaccharide injection. Thirty-two male 24-month-old C57BL/6 mice were subjected to the systemic injection of either saline (WT, $n = 8$; TG, $n = 8$) or lipopolysaccharide (LPS) (WT, $n = 3$; TG, $n = 13$). The aged WT and TG mice were injected intraperitoneally with sterile saline or *Escherichia coli* LPS (0.33 mg/kg; serotype 055:B5; Sigma-Aldrich). In the first study, mice ($n = 3$ for each group) were killed at 4 h after saline or LPS injection and the soluble extracts of the whole brain were subjected to the immunoblot analyses using anti-IL-1β antibody to measure the total IL-1β level. The mean relative immunoreactivity of IL-β was determined using expression of actin as an internal control. In a subsequent study, the immunofluorescence intensity of IL-1β/cell ($n = 3$ for each group), the immunofluorescence intensity of 8-oxo-dG/mitochondria ($n = 2$ for each group), and the magnitude of the long-term potentiation (LTP) were evaluated in the hippocampus prepared from the aged TG mice that had been injected by LPS at 4 h earlier (TG, $n = 5$).

Electrophysiology. Twenty-eight male C57BL/6 mice (WT and TG) of the following age groups: young (2–4 months of age; WT, $n = 6$; TG, $n = 5$) and aged (19–22 months of age; WT, $n = 10$; TG, $n = 7$) were used in the electrophysiological study. The brain was removed rapidly and hippocampal slices were prepared by cutting 400-μm-thick sagittal sections using a microslicer (VT1000S; Leica) as described previously (Hayashi et al., 2006). Some mice were injected LPS (0.33 mg/kg; Sigma-Aldrich) intraperitoneally 4 h before recording. Field EPSPs evoked by stimulation of the Schaffer collateral pathway were recorded from the CA1 subfield. LTP was induced by tetanus stimulation consisting of a train of pulses of 1 s duration given at 25, 50, and 100 Hz. All data were captured using the PowerLab (Molecular Devices), and then they were digitized (5–20 kHz) and stored on the hard disk of a personal computer for off-line analysis using the Scope software program.

Statistical analysis. Data are expressed as the mean ± SEM. The statistical analyses were performed by an ANOVA.

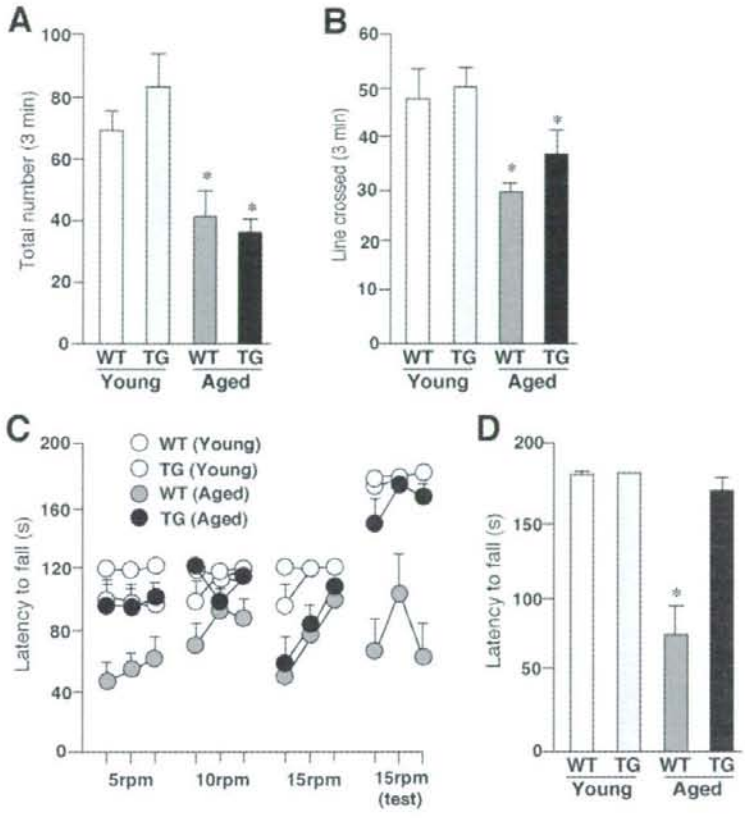

Figure 4. The amelioration of aged-dependent impairment of coordinated movements in the aged TG mice. ***A***, The mean total number of forepaw contacts. Each column and bar represent the mean ± SEM of six animals. The asterisks indicate significant differences versus the young group (*$p < 0.05$). ***B***, The mean incidence of line crossed. Each column and bar represent mean ± SEM of six animals. The asterisks indicate significant differences versus the young group (*$p < 0.05$). ***C***, The mean latency to fall from the rod given three practice trials at constant speed of 5 rpm in the first day, 10 and 15 rpm in the second day, and 15 rpm in the third (test) day. Each circle and bar represent the mean ± SEM of six animals. ***D***, The mean latency to fall from the rod in the test session (3 trials at 15 rpm). Each column and bar represents the mean ± SEM of six animals. An asterisk indicates a significant difference versus the young group (*$p < 0.05$).

Results

Inhibitory effect of TFAM overexpression on rotenone-induced intracellular ROS generation and NF-κB nuclear translocation in HeLa cells

TFAM overexpression may inhibit the ROS generation through reduction of mtDNA mutations, which subsequently retards the motor and memory functions. To elucidate this deduction, the effects of TFAM on intracellular ROS generation were first examined in HeLa cells overexpressing human TFAM using the tetracycline-off system. The protein level of TFAM in the HeLa cells increased approximately twofold by removal of DC, a derivative of tetracycline, from the culture medium (Fig. 1). Rotenone, an inhibitor of mitochondrial complex I, was used to produce ROS, which originated from the mitochondria, because impaired electrons transfer at complex I has been reported to be associated with an increased production of superoxide radicals (Hensley et al., 2000). Rotenone induced a significant increase in the oxidation level of DHE, a widely used ROS-sensitive dye (Fig. 2*A*,*B*). The mean oxidation level of rotenone-treated HeLa cells was significantly lower when cultured without DC than when cultured with DC. The effect of rotenone on the subsequent activation of NF-κB, a redox-sensitive nuclear transcription factor, was further examined in the HeLa cells overexpressing human TFAM by the tetracycline-off system. The activation of NF-κB in HeLa cells was assessed by visualizing its translocation from the cytoplasm to the nucleus after treatment with rotenone. Rotenone

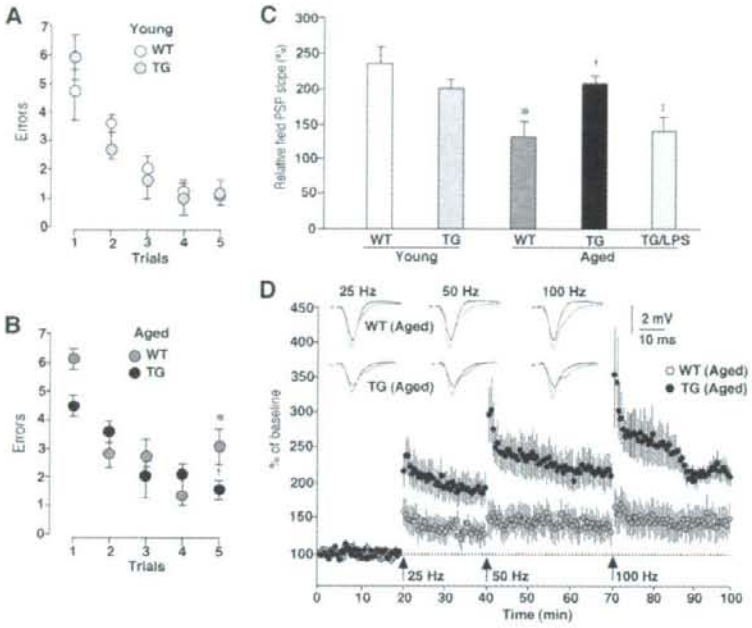

Figure 5. An amelioration of age-dependent decline of the working memory and the hippocampal LTP in the aged TG mice. ***A***, ***B***, The mean number of errors during radial-arm water maze performance in the TG and WT mice of both the young (***A***) and the aged groups (***B***). Four consecutive acquisition trials (trials 1–4) followed by a 30 min retention trial (trial 5) were conducted. Each circle and bar represents the mean ± SEM of six experiments. An asterisk indicates a significant difference versus the young WT mice ($^{*}p < 0.05$). A dagger indicates a significant difference versus the aged WT mice ($^{\dagger}p < 0.05$). ***C***, The mean relative EPSP slopes measured at 30 min after tetanic stimulation at 100 Hz in the Schaffer collateral–CA1 pathway of the WT and TG mice of both age groups and LPS-treated aged TG mice. Each column and bar represent the mean ± SEM of six slices from three animals in the young WT group, three slices from three animals in the young TG group, three slices from three animals in the aged WT group, 11 slices from seven animals in the aged TG group, and 15 slices from five animals in the aged TG group subjected to intraperitoneally injection of LPS (0.33 mg/kg) 4 h earlier. An asterisk indicates a significant difference versus the young WT mice ($^{*}p < 0.05$). A dagger indicates a significant difference versus the aged WT mice ($^{\dagger}p < 0.05$). A double dagger indicates a significant difference from the value of the aged TG mice ($^{\ddagger}p < 0.05$). ***D***, The cumulative potentiation of EPSP slope after consecutive tetanic stimulation at 25, 50, and 100 Hz in the hippocampus of aged WT and TG mice. Each circle and bar represent the mean ± SEM of three slices from three animals in the aged WT group, and 11 slices from seven animals in the aged TG group. The traces show the typical field EPSP before (black) and after stimulation at each frequency (gray).

also induced the NF-κB nuclear translocation in HeLa cells cultured with DC. However, the mean ratio of translocated NF-κB in rotenone-treated HeLa cells was significantly lower when they were cultured without DC than when they were cultured with DC (Fig. 2*C*;*D*, arrowheads). These results clearly indicate that the overexpression of TFAM prevents the overproduction of ROS originated from the mitochondria and inhibits the intracellular redox-sensitive signaling of NF-κB.

Amelioration of age-dependent increased oxidative stress and reduced activity of mitochondrial respiratory enzymes in the brain of aged TG mice

Next, the effect of TFAM overexpression on the ROS generation in the brain was examined using TG mice and their wild-type littermates. In the young TG mice, the human TFAM protein was expressed in the soluble extracts prepared from the whole brain, without any significant changes in the expression of the endogenous mouse Tfam protein (Fig. 3*A*). Immunostaining also showed human TFAM to be expressed in both neurons and glial cells in the brain parenchyma of the TG mice (Fig. 3*B*). Lipid peroxidation, which was indicated by TBARS, significantly increased in the brain tissue specimens of the aged WT mice. The increased lipid peroxidation may therefore contribute to the senescent changes in the brain functions. However, the mean TBARS level in the brain tissues of the aged TG mice was significantly lower than that in the aged WT mice and comparable with that in the young group (Fig. 3*C*). Many studies have suggested a mechanistic link between mtDNA mutations, a loss of mitochondrial respiratory enzyme functions, and generation of ROS from the mitochondria. A decreased electron transfer activity has been observed in the mitochondria of experimental animals on aging (Navarro et al., 2005; Mao et al., 2006). The activity of complexes I and IV in the mitochondrial fractions prepared from the brain tissue specimens of the aged WT mice were significantly lower compared with the young WT mice, whereas those of complexes II and III were unaffected (Fig. 3*D*). These results are consistent with those of previous reports (Navarro et al., 2005; Mao et al., 2006). In the brain tissue specimens prepared from the TG mice, however, there was no age-dependent reduction in activity for any of the complexes (Fig. 3*D*). Therefore, the age-dependent decrease in enzymatic activities of complexes I and IV could be mainly a consequence of oxidative mtDNA damage. Furthermore, it is reasonable to consider that human TFAM effectively counteracted this oxidative mtDNA damage to rescue the age-dependent decrease in mitochondrial complex enzymatic activities.

Amelioration of the aged-dependent impairment of motor learning and memory in aged TG mice

The effects of TFAM overexpression were next observed regarding the age-dependent impairment of the locomotor activity and the motor learning and memory using rotarod tests, because ROS are considered to be a major causal factor for the progressive age-dependent motor and learning functions.

The locomotor activities were measured by both the cylinder and line-crossing tests. The mean total number of both forepaw contacts and the incidence of line crossed significantly decreased with aging in both the WT and TG mice (Fig. 4*A*,*B*). The mean total number of forepaw contacts showed no significant difference between the aged WT mice and the aged TG mice (Fig. 4*A*). All groups of animals used in this study had an equal forelimb use. The mean total incidence of line crossed in the aged TG mice was larger than that in the aged WT mice, whereas the difference did not reach the statistical significance (Fig. 4*B*).

Next, the rotarod test was used to examine the effects of TFAM overexpression on the age-dependent impaired acquisition of skilled behavior. With the fixed speed rotarod protocol, both the young WT and TG mice could rapidly acquire the necessary skilled behavior on the rotating rod to prevent a fall. They were able to stay on the rod for the maximum time at both trained at speeds between 5 and 15 rpm and tested at 15 rpm (Fig. 4*C*). The aged WT mice showed an increase in the latency to fall across trials, but their score was much lower than that of the young

group. During the test session, the average time spent on the rod significantly decreased with aging in the WT mice (Fig. 4*D*). Furthermore, regardless of the progress during three trials at 15 rpm, the aged WT mice fell down from the rod in ~60 s in the first trial in the test session on the next day (Fig. 4*C*,*D*). However, the aged TG mice could rapidly acquire the skilled behavior on the rotating rod similar to the young group at speeds with 5 and 10 rpm (Fig. 4*C*). In the task at a speed of 15 rpm, the aged TG mice showed a slow acquisition of the skilled behavior compared with the young group. Because of the fact that the mice had to turn their position against the direction of rotation and progress forward to maintain their equilibrium on the rod after the rod started to rotate, they needed to acquire the more skillful behavior at higher speeds. During the test session, however, the mean latency to fall of the aged TG mice significantly increased compared with that of the aged WT mice (Fig. 4*D*). Although the aged WT animals could not reach the maximum time during the test session for their low endurance, they stayed on the rod for more than their maximum time during the fixed speed protocol and at speed >15 rpm in the accelerating rotarod protocol (accelerate continuously from 4 to 40 rpm over 300 s) (data not shown). In addition, there was no difference in locomotive activation between WT and TG mice (Fig. 4*A*,*B*), thus suggesting that a decrease in the time spent on the rod was caused by an impairment of the acquisition of the skilled behavior rather than by a decline in their endurance or motivation. These results indicate that the age-dependent motor memory impairment markedly improved in the TG mice.

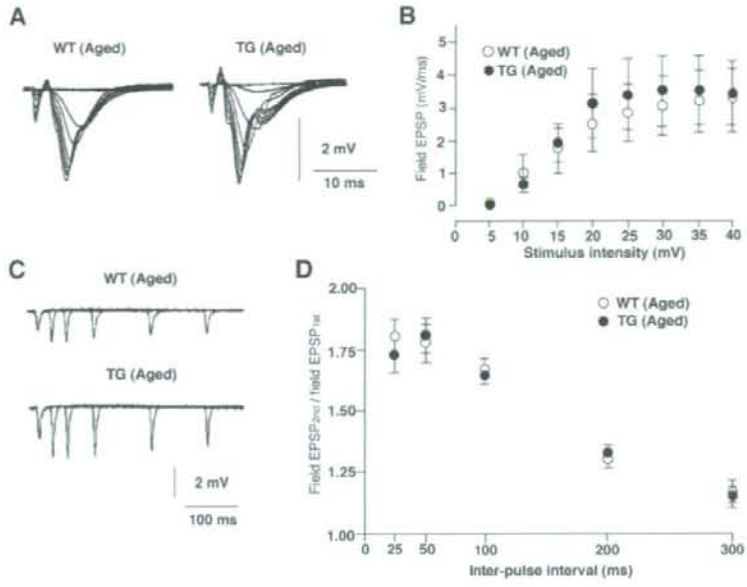

Figure 6. Effects of TFAM overexpression on basal synaptic transmission in the hippocampus. ***A***, Superimposed traces of field EPSPs evoked by different stimulus intensities (5–40 V) from the CA1 subfield of hippocampal slices prepared from the aged WT and TG mice. ***B***, The input–output relationship for the mean field EPSP slope plotted against stimulus intensity in the Schaffer collateral–CA1 synapses. Open circles, WT mice; filled circles, TG mice. The point and bar represent the mean and SEM of eight slices from eight animals in the aged WT group, and seven slices from three animals in the aged TG group. No significant difference was observed between the WT and TG slices. ***C***, Superimposed traces of field EPSPs evoked by paired pulse stimulation of the stratum radiatum with five different interspike intervals in the CA1 subfield of hippocampal slices prepared from the aged WT and TG mice. ***D***, The plots of the relative amplitude of the second stimulation to the first responses against various interstimulus intervals. Open circles, WT mice; filled circles, TG mice. The point and bar represent the mean and SEM of six to eight slices from six animals in the aged WT mice, and seven slices from seven animals in aged TG mice. No significant difference was observed between WT and TG slices.

Amelioration of the age-dependent decline of the working memory and the hippocampal LTP in the aged TG mice

Next, the effects of TFAM overexpression on the age-dependent impairment of the working memory were examined using the radial arm water maze, which combines elements of a radial-arm maze and a water maze (Morgan et al., 2000). Both the WT and TG mice of the young group showed an average of four to six errors in the first trial and only one error in the retention trial (trial 5) (Fig. 5*A*). In both the WT and TG mice of the aged group, the animals showed four to six errors on the first trial. On the retention trial (trial 5), the mean number of errors in the aged TG mice was significantly lower than that in the aged group and it was comparable with that in the young group (Fig. 5*B*).

These observations prompted the additional examination of the effects of TFAM overexpression on the age-dependent decline in the hippocampal LTP, which is postulated to be a cellular substrate for hippocampus-dependent memory. The LTP experiments were performed on transverse hippocampal slices as described previously (Tomimatsu et al., 2002; Hayashi et al., 2006). The cumulative potentiation of the field EPSP slope was measured after consecutive tetanic stimulation at 25, 50, and 100 Hz. When the relative field EPSP slope was measured at 30 min after tetanic stimulation with 100 Hz, there was no significant difference in the mean magnitude of LTP in the Schaffer collateral–CA1 pathway between the young WT and TG mice (Fig. 5*C*). Consistent with previous studies (Okada et al., 1995), LTP in the Schaffer collateral–CA1 pathway was significantly lower in the aged WT mice than in the young WT mice (Fig. 5*C*). However, LTP was induced by conditioned stimuli even at a relatively low frequency (25 or 50 Hz) in the aged TG mice (Fig. 5*D*). The mean relative field EPSP slope measured at 30 min after tetanic stimulation with 100 Hz in the aged TG mice was significantly greater than that in the aged WT mice and it was also comparable with that in the young group (Fig. 5*C*,*D*).

However, there was no significant difference in either the basal synaptic transmission (Fig. 6*A*,*B*) or the paired-pulse facilitation (Fig. 6*C*,*D*) between the aged WT and TG mice. These results clearly indicate that an overexpression of TFAM significantly ameliorates the age-dependent deficits in the working memory and the hippocampal LTP.

Amelioration of increased oxidation and inflammation in the brain of the aged TG mice

ROS have been associated with normal aging and age-dependent neurodegenerative disorders (Watson et al., 2006). The localization of oxidative damages was examined in the hippocampus and other brain regions. The immunoreactivity for HNE and 8-oxodG, which are formed by oxidant interactions with lipids and DNA, respectively, increased in the aged WT mouse brains. In-

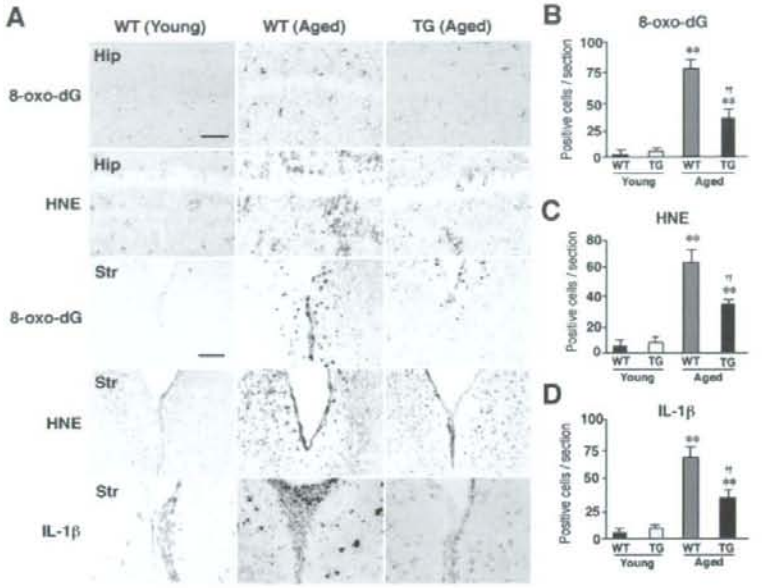

Figure 7. Amelioration of ROS-mediated oxidation of cell components and inflammation in the hippocampus of the aged TG mice. ***A***, Immunohistochemical staining for 8-oxo-dG and HNE in the CA1 hippocampal subfield (Hip) and the periventricular area of the striatum (Str) of the young WT, the aged WT, and the aged TG mice. Scale bars, 50 μm. ***B–D***, The mean number of positive cells for 8-oxo-dG (***B***), HNE (***C***), and IL-1β/cells (***D***) in the hippocampal CA1 subfield of the WT, the TG, and the LPS-treated TG mice of the aged group. Each column and bar represent the mean ± SEM of nine sections from three animals. The asterisks indicate significant differences versus the young group (**$p < 0.01$). The daggers indicate significant differences versus the aged WT mice ($^{\dagger\dagger}p < 0.01$).

creased immunoreactivity was prominent especially in the hippocampus and the periventricular areas of the striatum (Fig. 7*A–C*). In contrast, the immunoreactivity of these markers for oxidative stress was barely detectable in the brain parenchyma of the aged TG mice (Fig. 7*A–C*). The immunoreactivity for IL-1β also significantly increased in the periventricular areas (Fig. 7*A*,*D*) and the hippocampus (data not shown) of the aged WT mice but not those brain regions of the aged TG mice. Double immunofluorescence staining was performed to elucidate the cellular sources for 8-oxo-dG, HNE, and IL-1β. Rather surprisingly, the immunoreactivity for both 8-oxo-dG and HNE corresponded closely with microglia exhibiting activated morphology and partially with neurons, but not with astrocytes localized in the periventricular area of the aged WT mice (Fig. 8*A*,*B*). The relatively intense immunoreactivity for IL-1β corresponded well with that for both Iba1 and GFAP, but not MAP2 in the periventricular areas (Fig. 8*C*) and the hippocampus (Fig. 9*C*) of the aged WT mice. In the hippocampus of the aged WT mice, the immunoreactivity for either 8-oxo-dG (Fig. 8*D*, red) or HNE (data not shown) was found mainly in glial cells and only partially in neurons that were intensely stained with YOYO-1 (green). The immunoreactivity for 8-oxo-dG (Fig. 8*F*) and HNE (Fig. 8*G*) found in the stratum radiatum corresponded well with microglia. However, the immunoreactivity for either 8-oxo-dG (Fig. 8*E*) or HNE (data not shown) was barely detectable in the hippocampus of the aged TG mice.

Recent accumulating evidence indicates that intracellular ROS is capable of activating redox-dependent signal transduction cascades and transcription factors including NF-κB and mitogen-activated protein (MAP) kinases in various cell types including microglia (Pawate et al., 2004; Yamasaki et al., 2007). The activation of NF-κB and MAP kinases is closely associated with the expression of inflammatory mediators including IL-1β in microglia. Furthermore, inflammatory mediators including IL-1β secreted from microglia have been recently reported to play a pivotal role in the attenuation of the working memory (Gemma et al., 2005) and the hippocampal LTP in aged rats (Griffin et al., 2006). Therefore, the relationship between the oxidative damage of mtDNA, the expression level of IL-1β, and the magnitude of the hippocampal LTP was examined by treatment with LPS, which is known to increase the generation of mitochondrial ROS (Woo et al., 2004; Emre et al., 2007). At 4 h after the systemic injection of LPS, the mean level of IL-1β in the whole brain of the aged TG mice significantly increased, thus reaching a similar level to that of the aged WT mice (Fig. 9*A*,*B*). However, the mean level of IL-1β in the whole brain of the LPS-treated aged TG mice was significantly lower that of the LPS-treated aged WT mice (Fig. 9*A*,*B*). However, the immunoreactivity for 8-oxo-dG corresponded closely with that for Cyt *b*, a marker for the mitochondria, was observed in the hippocampus of the aged WT mice. In contrast, there was slight immunoreactivity for either IL-1β or 8-oxo-dG in the hippocampus of the aged TG mice. On treatment with LPS, the immunoreactivity for both IL-1β and 8-oxo-dG markedly increased in the hippocampus of the aged TG mice (Fig. 9*C*). The immunoreactive products for IL-1β showed a specked appearance, thus suggesting the localization of IL-1β in lysosomes where IL-1β colocalizes with lysosomal enzymes (Gardella et al., 2001; Qu et al., 2007). The mean immunofluorescence intensity of IL-1β/cell in the hippocampus of the LPS-treated aged TG mice was significantly higher than that in the aged TG mice and it was also comparable with that in the aged WT mice (Fig. 9*C*,*D*). At the same time, the mean immunofluorescence intensity of 8-oxo-dG/mitochondria in the hippocampus of the LPS-treated aged TG mice was also significantly higher than that in the aged TG mice (Fig. 9*C*,*E*). Finally, LTP in the Schaffer collateral–CA1 pathway was measured in hippocampal slices prepared from the LPS-treated aged TG mice. As shown in Figure 5*C*, the mean magnitude of LTP in the LPS-treated aged TG mice was significantly lower than that of none-treated aged TG mice (143.86 ± 10.17%; $p < 0.05$).

These observations strongly suggest that overexpressed human TFAM also significantly suppressed mitochondrial ROS generation and the subsequent IL-1β production by microglia in the brain. Furthermore, the magnitude of the hippocampal LTP was inversely correlated with the expression level of IL-1β and the severity of mtDNA damage in microglia.

Discussion

The mitochondrial theory of aging states that the original damage to mtDNA is induced by the continuous production of ROS (Beckman and Ames, 1998; Harman, 2006). The most important

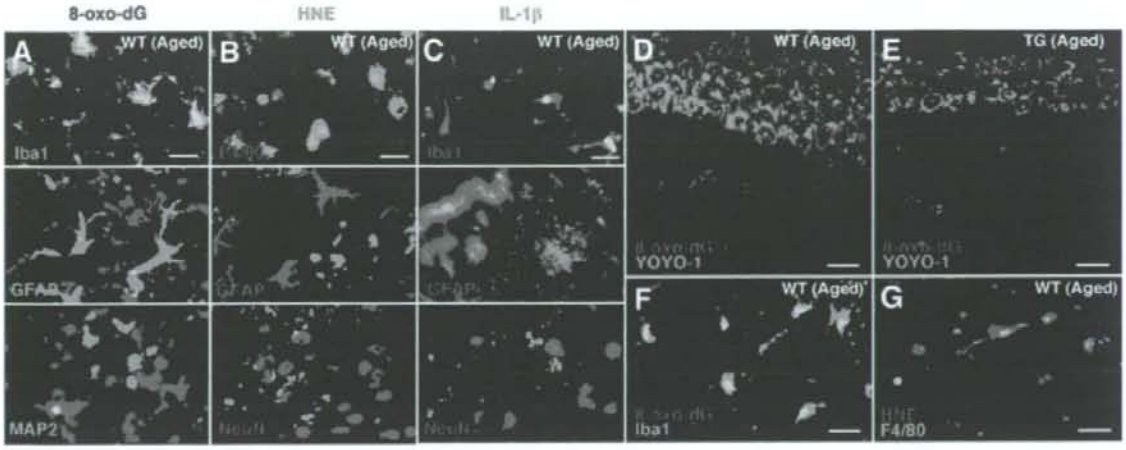

Figure 8. Immunofluorescent CLSM images for 8-oxo-dG, HNE, and IL-1β in the striatum and the hippocampus. ***A–C***, Immunofluorescence for 8-oxo-dG (***A***), HNE (***B***), and IL-1β (***C***) with cell type markers (Iba1, F4/80 for microglia, GFAP for astrocytes, MAP2 and NeuN for neurons) in the periventricular area of the striatum of the aged WT mice. Scale bars: ***A–C***, 30 μm. ***D***, ***E***, Immunofluorescence for 8-oxo-dG (red) with YOYO-1-stained neurons (green) in the hippocampal CA1 subfield of the aged WT (***D***) and TG (***E***) mice. Scale bars: ***D***, ***E***, 20 μm. ***F***, ***G***, Immunofluorescence for 8-oxo-dG (***F***) and HNE (***G***) with markers of microglia (Iba1 and F4/80) in the hippocampal CA1 subfield of the aged WT mice. Scale bars: ***F***, ***G***, 5 μm.

finding in the current study is that the overexpression of human TFAM reduced age-dependent oxidative damages of mtDNA mainly in microglia, thus preventing the age-dependent impairments in the motor and working memories in mice. These beneficial effects of human TFAM overexpression were attributable to functional improvements in the brain but not in the musculature in the aged TG mice. Considering (1) the abundance of TFAM, (2) the structure of TFAM as high-mobility group DNA-binding protein, and (3) the association of TFAM with mtDNA protein complexes (Alam et al., 2003; Kanki et al., 2004a; Kang and Hamasaki, 2005), (4) human TFAM dose not appear to work as a transcription factor in a mouse cell (Ohgaki et al., 2007), human TFAM can cover the whole region of a mtDNA forming nucleoid to protect it from oxidative modifications or additional damage without modulation of gene expression (Kanki et al., 2004a; Kang and Hamasaki, 2005). The present study clearly demonstrated a causal relationship among mitochondrial ROS, mitochondrial dysfunction, and deficits in the brain functions during the process of aging.

The results of this study revealed that microglia are the main cellular source of oxidation products including HNE and 8-oxo-dG in the brain of the WT mice. It was also noted that the accumulation of oxidation products in microglia was more marked in specific brain areas including the hippocampus and the periventricular area of the striatum. These marked oxidative stresses on microglia in the hippocampus and striatum are considered to be closely associated with the age-dependent memory deficits, because these brain regions play key roles in the formation of motor and working memories, respectively (Morris et al., 1982; Albin et al., 1989). These observations remain, however, somewhat puzzling because the most severe age-dependent mtDNA injury and greatest ROS production in the brain are believed to occur in neurons that are long-living postmitotic cells. Liu et al. (2002) demonstrated RNA to be the predominant oxidized neuronal nucleic acid in the aged rat brain. Therefore, RNA being the predominant oxidized neuronal nucleic acid in the aged animal brain may explain the paucity of oxidative mtDNA damage in neurons of the aged WT mice in the present immunohistochemical analysis using anti-8-oxo-dG antibody. However, some evidence suggests that the mitochondrial turnover in microglia is extremely slow and that abundant damaged mitochondria, which can generate excessive ROS, may accumulate in microglia. A recent study showed the subunit c of the mitochondrial ATP synthase complex to accumulate most intensively in microglia in the brain of the mice deficient for cathepsin D, which is a protease responsible for proteolytic degradation of subunit c (Yamasaki et al., 2007). Furthermore, Lawson et al. (1992) revealed a slow microglial turnover in the normal adult mouse brain, although microglia are replaceable cells. The age-dependent changes in the mitochondrial functions and ROS production in microglia are thus expected to be elucidated in future studies.

The current observations showed that TFAM overexpression suppressed the ROS generation induced by rotenone and the subsequent activation of NF-κB in HeLa cells. ROS induced by rotenone were generated from the mitochondria because an impaired electron transfer at complex I is associated with an increased production of ROS in the mitochondria (Schönfeld and Reiser, 2006). Furthermore, a decrease in the enzymatic activity of complex I in the range of 16–30% is sufficient to stimulate mitochondrial ROS generation (Sipos et al., 2003). Therefore, a decrease in the activity of both complexes I and IV by approximately one-third in the brain of the aged WT mice could induce excessive mitochondrial ROS generation. These excess ROS may further cause oxidative DNA damage, lipid peroxidation, and IL-1β production through activation of NF-κB. Therefore, human TFAM overexpression may also reduce excessive mitochondrial ROS generation in the brain during aging and the subsequent oxidative damage and inflammatory responses through the protection of mtDNA against oxidative injury.

Although the observations noted herein showed that the systemic injection of LPS could further activate microglia to produce IL-1β in the brain of the aged TG mice, the mean amount of IL-1β in the brain of the LPS-treated aged TG mice was significantly lower than that of the LPS-treated aged WT mice. LPS is therefore suggested to activate microglia by a multitude of receptors and interacting pathways (Qin et al., 2005), with the production of ROS. Recently, mitochondria have been found to contribute to LPS-induced ROS signaling in macrophages (Woo et al.,

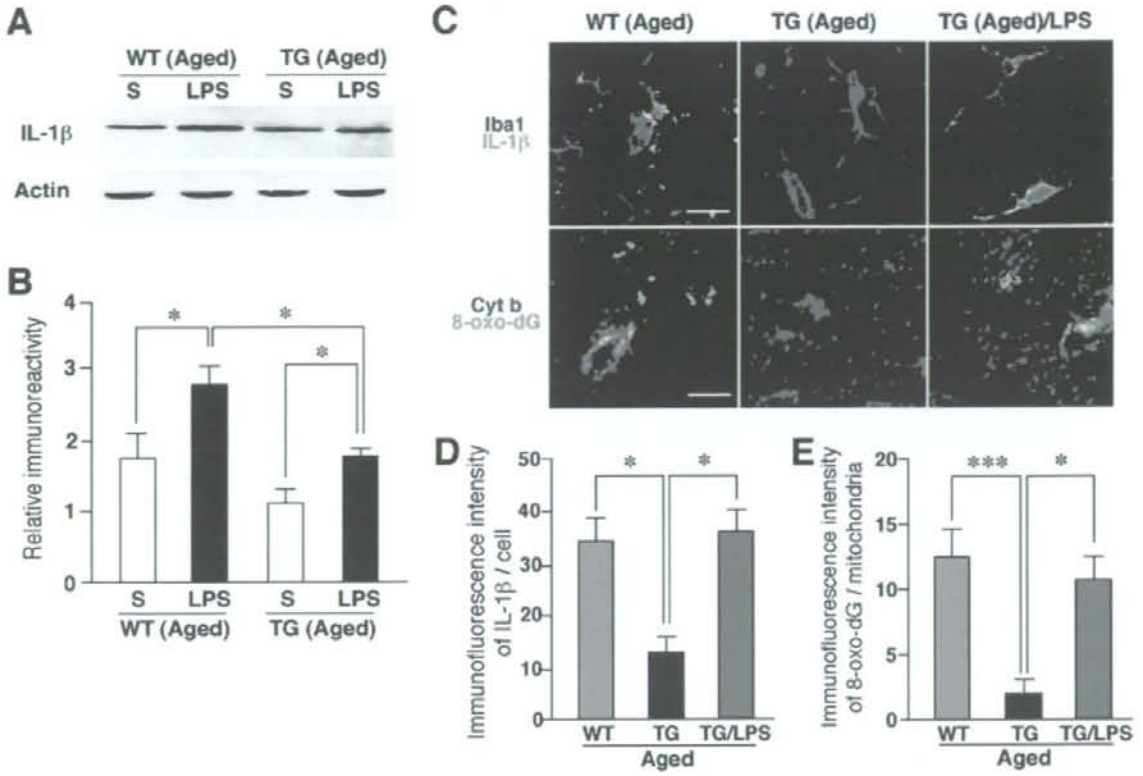

Figure 9. Increased expression of IL-1β in the hippocampus after the systemic injection of LPS and the inhibitory effect of the TFAM overexpression. ***A***, Immunoblot analysis of IL-1β in the whole brain of the aged WT and TG mice subjected to intraperitoneal injection of saline (S) or LPS (0.33 mg/kg) 4 h earlier. ***B***, The mean protein level of IL-1β. The mean relative immunoreactivity was determined using the level of actin as an internal control. Each column and bar represent the mean and SEM of three experiments, respectively. The asterisks indicate significant differences between the values (*$p < 0.05$). ***C***, Immunofluorescent CLSM images for IL-1β (green) with the microglial marker Iba1 (red; top row), and 8-oxo-dG (green) with the mitochondrial marker Cyt *b* (red; bottom row) in the hippocampal CA1 subfield of the aged WT, the aged TG, and the LPS-treated aged TG mice. Scale bars: top row, 10 μm; bottom row, 5 μm. ***D***, The mean immunofluorescence intensity of IL-1β/cell in the hippocampal CA1 subfield of the WT, the TG, and the LPS-treated TG mice of the aged group. Each column and bar represent the mean ± SEM of nine sections from three animals. The asterisks indicate significant differences between the values (*$p < 0.05$). ***E***, The mean immunofluorescence intensity of 8-oxo-dG/mitochondria in the hippocampal CA1 subfield of the WT, the TG, and the LPS-treated TG mice of the aged group. Each column and bar represent the mean ± SEM of seven sections from two animals. The asterisks indicate significant differences between the values (***$p < 0.0001$; *$p < 0.05$).

2004; Emre et al., 2007). It is therefore conceivable that the overexpression of TFAM also inhibited the LPS-induced mitochondrial ROS generation to reduce oxidative mtDNA damage and the IL-1β levels in the brain. There is increasing evidence that neuroinflammation mediated by activated microglia plays a major causative role in age-dependent deficit of the working memory (Gemma et al., 2005) and the hippocampal LTP (Griffin et al., 2006). It is therefore reasonable to consider that TFAM overexpression may inhibit any excessive ROS generation caused by a reduced mitochondrial respiratory chain enzymatic activity in microglia during aging, because ROS can activate NF-κB, which integrates oxidative stress and the inflammatory pathways (Pawate et al., 2004). Additional clarification of the mechanisms by which TFAM exhibits an antioxidant effect and maintains the mitochondrial function may eventually lead to the development of an antiaging strategy to preserve the brain functions.

References

Alam TI, Kanki T, Muta T, Ukaji K, Abe Y, Nakayama H, Takio K, Hamasaki N, Kang D (2003) Human mitochondrial DNA is packaged with TFAM. Nucleic Acids Res 31:1640–1645.

Albin RL, Young AB, Penney JB (1989) The functional anatomy of basal ganglia disorders. Trends Neurosci 12:366–375.

Beckman KB, Ames BN (1998) The free radical theory of aging matures. Physiol Rev 78:547–581.

Corral-Debrinski M, Horton T, Lott MT, Shoffner JM, Beal MF, Wallace DC (1992) Mitochondrial DNA deletions in human brain: regional variability and increase with advanced age. Nat Genet 2:324–329.

Emre Y, Hurtaud C, Nübel T, Criscuolo F, Ricquier D, Cassard-Doulcier AM (2007) Mitochondria contribute to LPS-induced MAPK activation via uncoupling protein UCP2 in macrophages. Biochem J 402:271–278.

Forster MJ, Dubey A, Dawson KM, Stutts WA, Lal H, Sohal RS (1996) Age-related losses of cognitive function and motor skills in mice are associated with oxidative protein damage in the brain. Proc Natl Acad Sci U S A 93:4765–4769.

Gardella S, Andrei C, Lotti LV, Poggi A, Torrisi MR, Zocchi MR, Rubartelli A (2001) CD8$^+$ T lymphocytes induce polarized exocytosis of secretory lysosomes by dendritic cells with release of interleukin-1β and cathepsin D. Blood 98:2152–2159.

Gemma C, Fister M, Hudson C, Bickford PC (2005) Improvement of memory for context by inhibition of caspase-1 in aged rats. Eur J Neurosci 22:1751–1756.

Griffin R, Nally R, Nolan Y, McCartney Y, Linden J, Lynch MA (2006) The

age-related attenuation in long-term potentiation is associated with microglial activation. J Neurochem 99:1263–1272.
Harman D (2006) Free radical theory of aging: an update: increasing the functional life span. Ann N Y Acad Sci 1067:10–21.
Hayashi Y, Tomimatsu Y, Suzuki H, Yamada J, Wu Z, Yao H, Kagamiishi Y, Tateishi N, Sawada M, Nakanishi H (2006) The intra-arterial injection of microglia protects hippocampal CA1 neurons against global ischemia-induced functional deficits in rats. Neuroscience 142:87–96.
Hensley K, Kotake Y, Sang H, Pye QN, Wallis GL, Kolker LM, Tabatabaie T, Stewart CA, Konishi Y, Nakae D, Floyd RA (2000) Dietary choline restriction causes complex I dysfunction and increased H_2O_2 generation in liver mitochondria. Carcinogenesis 21:983–989.
Iancu R, Mohapel P, Brundin P, Paul G (2005) Behavioral characterization of a unilateral 6-OHDA-lesion model of Parkinson's disease in mice. Behav Brain Res 162:1–10.
Ide T, Tsutsui H, Kinugawa S, Utsumi H, Kang D, Hattori N, Uchida K, Arimura K, Egashira K, Takeshita A (1999) Mitochondrial electron transport complex I is a potential source of oxygen free radicals in the failing myocardium. Circ Res 85:357–363.
Ikeuchi M, Matsusaka H, Kang D, Matsushima S, Ide T, Kubota T, Fujiwara T, Hamasaki N, Takeshita A, Sunagawa K, Tsutsui H (2005) Overexpression of mitochondrial transcription factor A ameliorates mitochondrial deficiencies and cardiac failure after myocardial infarction. Circulation 112:683–690.
Kajitani K, Yamaguchi H, Dan Y, Furuichi M, Kang D, Nakabeppu Y (2006) MTH1, an oxidized purine nucleoside triphosphatase, suppresses the accumulation of oxidative damage of nucleic acids in the hippocampal microglia during kainate-induced excitotoxicity. J Neurosci 26:1688–1698.
Kang D, Hamasaki N (2005) Mitochondrial transcription factor A in the maintenance of mitochondrial DNA: overview of its multiple roles. Ann N Y Acad Sci 1042:101–108.
Kanki T, Nakayama H, Sasaki N, Takio K, Alam TI, Hamasaki N, Kang D (2004a) Mitochondrial nucleoid and transcription factor A. Ann N Y Acad Sci 1011:61–68.
Kanki T, Ohgaki K, Gaspari M, Gustafsson CM, Fukuoh A, Sasaki N, Hamasaki N, Kang D (2004b) Architectural role of mitochondrial transcription factor A in maintenance of human mitochondrial DNA. Mol Cell Biol 24:9823–9834.
Lawson LJ, Perry VH, Gordon S (1992) Turnover of resident microglia in the normal adult mouse brain. Neuroscience 48:405–415.
Lin MT, Simon DK, Ahn CH, Kim LM, Beal MF (2002) High aggregate burden of somatic mtDNA point mutations in aging and Alzheimer's disease brain. Hum Mol Genet 11:133–145.
Liu J, Head E, Gharib AM, Yuan W, Ingersoll RT, Hagen TM, Cotman CW, Ames BN (2002) Memory loss in old rats is associated with brain mitochondrial decay and RNA/DNA oxidation: partial reversal by feeding acetyl-L-carnitine and/or R-α-lipoic acid. Proc Natl Acad Sci U S A 99:2356–2361.
Mao L, Zabel C, Wacker MA, Nebrich G, Sagi D, Schrade P, Bachmann S, Kowald A, Klose J (2006) Estimation of the mtDNA mutation rate in aging mice by proteome analysis and mathematical modeling. Exp Gerontol 41:11–24.
Morgan D, Diamond DM, Gottschall PE, Ugen KE, Dickey C, Hardy J, Duff K, Jantzen P, DiCarlo G, Wilcock D, Connor K, Hatcher J, Hope C, Gordon M, Arendash GW (2000) Aβ peptide vaccination prevents memory loss in an animal model of Alzheimer's disease. Nature 408:982–985.
Morris RG, Garrud P, Rawlins JN, O'Keefe J (1982) Place navigation impaired in rats with hippocampus lesions. Nature 297:681–683.
Navarro A, Sánchez Del Pino MJ, Gómez C, Peralta JL, Boveris A (2002) Behavioral dysfunction, brain oxidative stress, and impaired mitochondrial electron transfer in aging mice. Am J Physiol Regul Integr Comp Physiol 282:R985–R992.
Navarro A, Gomez C, López-Cepero JM, Boveris A (2004) Beneficial effects of moderate exercise on mice aging: survival, behavior, oxidative stress, and mitochondrial electron transfer. Am J Physiol Regul Integr Comp Physiol 286:R505–R511.
Navarro A, Gómez C, Sánchez-Pino MJ, González H, Bández MJ, Boveris AD, Boveris A (2005) Vitamin E at high doses improves survival, neurological performance, and brain mitochondrial function in aging male mice. Am J Physiol Regul Integr Comp Physiol 289:R1329–R1399.
Ohgaki K, Kanki T, Fukuoh A, Kurisaki H, Aoki Y, Ikeuchi M, Kim SH, Hamasaki N, Kang D (2007) The C-terminal tail of mitochondrial transcription factor A markedly strengthens its general binding to DNA. J Biochem 141:201–211.
Okada M, Nakanishi H, Tamura A, Urae A, Mine K, Yamamoto K, Fujiwara M (1995) Long-term spatial cognitive impairment after middle cerebral artery occlusion in rats: no involvement of the hippocampus. J Cereb Blood Flow Metab 15:1012–1021.
Parisi MA, Clayton DA (1991) Similarity of human mitochondrial transcription factor 1 to high mobility group proteins. Science 252:965–969.
Pawate S, Shen Q, Fan F, Bhat NR (2004) Redox regulation of glial inflammatory response to lipopolysaccharide and interferon γ. J Neurosci Res 77:540–551.
Qin L, Li G, Qian X, Liu Y, Wu X, Liu B, Hong JS, Block ML (2005) Interactive role of the Toll-like receptor 4 and reactive oxygen species in LPS-induced microglia activation. Glia 52:78–84.
Qu Y, Franchi L, Nunez G, Dubyak GR (2007) Nonclassical IL-1β secretion stimulated P2X7 receptors is dependent on inflammasome activation and correlated with exosome release in murine macrophages. J Immunol 179:1913–1925.
Schönfeld P, Reiser G (2006) Rotenone-like action of the branched-chain phytanic acid induces oxidative stress in mitochondria. J Biol Chem 281:7136–7142.
Sipos I, Tretter L, Adam-Vizi V (2003) Quantitative relationship between inhibition of respiratory complexes and formation of reactive oxygen species in isolated nerve terminals. J Neurochem 84:112–118.
Tillerson JL, Cohen AD, Caudle WM, Zigmond MJ, Schallert T, Miller GW (2002) Forced nonuse in unilateral parkinsonian rats exacerbates injury. J Neurosci 22:6790–6799.
Tomimatsu Y, Idemoto S, Moriguchi S, Watanabe S, Nakanishi H (2002) Proteases involved in long-term potentiation. Life Sci 72:355–361.
Watson JB, Arnold MM, Ho YS, O'Dell TJ (2006) Age-dependent modulation of hippocampal long-term potentiation by antioxidant enzymes. J Neurosci Res 84:1564–1574.
Woo CH, Lim JH, Kim JH (2004) Lipopolysaccharide induces matrix metalloproteinase-9 expression via a mitochondrial reactive oxygen species-p38 kinase-activator protein-1 pathway in raw 264.7 cells. J Immunol 173:6973–6980.
Yamasaki R, Zhang J, Koshiishi I, Sastradipura Suniarti DF, Wu Z, Peters C, Schwake M, Uchiyama Y, Kira J, Saftig P, Utsumi H, Nakanishi H (2007) Involvement of lysosomal storage-induced p38 MAP kinase activation in the overproduction of nitric oxide by microglia in cathepsin D-deficient mice. Mol Cell Neurosci 35:573–584.

Human Molecular Genetics, 2008, Vol. 17, No. 17 **2654–2664**
doi:10.1093/hmg/ddn165
Advance Access published on June 10, 2008

Regulation of DNA methylation activity through *Dnmt3L* promoter methylation by Dnmt3 enzymes in embryonic development

Ye-Guang Hu[1], Ryutaro Hirasawa[2,3], Jia-Lei Hu[1], Kenichiro Hata[4], Chun-Liang Li[5], Ying Jin[5], Taiping Chen[6], En Li[6], Muriel Rigolet[7], Evani Viegas-Péquignot[7], Hiroyuki Sasaki[2,3] and Guo-Liang Xu[1,*]

[1]The State Key Laboratory of Molecular Biology, Institute of Biochemistry and Cell Biology, Shanghai Institutes for Biological Sciences, Chinese Academy of Sciences, 320 Yueyang Road, Shanghai 200031, People's Republic of China, [2]Department of Integrated Genetics, Division of Human Genetics, National Institute of Genetics, Research Organization of Information and Systems (ROIS), Mishima, Japan, [3]Department of Genetics, School of Life Science, The Graduate University for Advanced Studies (SOKENDAI), Mishima, Japan, [4]Department of Maternal-Fetal Biology, National Center for Child Health and Development, 2-10-1 Okura, Setagaya, Tokyo 157-8535, Japan, [5]Institute of Health Science, Shanghai JiaoTong University School of Medicine and Shanghai Institutes for Biological Sciences, Chinese Academy of Sciences, 225 South Chongqing Road, Shanghai 200025, People's Republic of China, [6]Epigenetics Program, Novartis Institutes for Biomedical Research, Cambridge, USA and [7]U741 Inserm/ Université Paris Diderot - Paris 7, 2 place Jussieu, Tour 43, 2ème étage, couloir 43-44, 75251 Paris cedex 05, France

Received February 1, 2008; Revised and Accepted May 28, 2008

The genomic DNA is methylated by *de novo* methyltransferases Dnmt3a and Dnmt3b during early embryonic development. The establishment of appropriate methylation patterns depends on a fine regulation of the methyltransferase activity. The activity of both enzymes increases in the presence of Dnmt3L, a Dnmt3a/3b-like protein. However, it is unclear how the function of Dnmt3L is regulated. We found here that the expression of Dnmt3L is controlled via its promoter methylation during embryonic development. Genetic studies showed that Dnmt3a, Dnmt3b and Dnmt3L are all involved in the methylation of the *Dnmt3L* promoter. Disruption of both *Dnmt3a* and *Dnmt3b* genes in mouse rendered the *Dnmt3L* promoter devoid of methylation, causing incomplete repression of the *Dnmt3L* transcription in embryonic stem cells and embryos. Disruption of either *Dnmt3a* or *Dnmt3b* led to reduced methylation and increased transcription of *Dnmt3L*, but severe hypomethylation occurred only when Dnmt3b was deficient. Consistent with the major contribution of Dnmt3b in the *Dnmt3L* promoter methylation, methylation of *Dnmt3L* was significantly reduced in mouse models of the human ICF syndrome carrying point mutations in *Dnmt3b*. Interestingly, Dnmt3L also contributes to the methylation of its own promoter in embryonic development. We thus propose an auto-regulatory mechanism for the control of DNA methylation activity whereby the activity of the *Dnmt3L* promoter is epigenetically modulated by the methylation machinery including Dnmt3L itself. Insufficient methylation of the *DNMT3L* promoter during embryonic development due to deficiency in *DNMT3B* might be implicated in the pathogenesis of the ICF syndrome.

*To whom correspondence should be addressed. Tel: +86 2154921332; Fax: +86 2154921266; Email: glxu@sibs.ac.cn

INTRODUCTION

Methylation of cytosines is the only known genome modification in vertebrates. Formation of cell-type-specific genomic methylation patterns is thought to be one of the underlying mechanisms for the differential programming of cell lineages. Cytosine methylation is required in various biological processes such as X-chromosome inactivation, genomic imprinting, transposon silencing and the regulation of tissue-specific gene expression. Aberrant DNA methylation contributes to many human diseases, including cancer (1,2).

DNA methylation patterns are established mainly during embryonic development, through highly regulated processes of *de novo* methylation and demethylation (3). Afterwards, they are stably maintained by the action of the maintenance methyltransferase Dnmt1 (4). The *de novo* methylation is carried out by three members of the Dnmt3 family. Dnmt3a and Dnmt3b are the two functional *de novo* methyltransferases with various isoforms. They are highly expressed in embryonic stem (ES) cells, early embryos and developing germ cells, but in differentiated cells only the longer isoform of Dnmt3a is expressed (5–8). In human, mutations in *DNMT3B* cause the ICF syndrome characterized by immunodeficiency, centromere instability and facial anomalies (6,9,10). Defective methylation at the classical satellites is a genomic hallmark of ICF patients. Dnmt3L is the third member of the Dnmt3 family. It shares homology with Dnmt3a and Dnmt3b but lacks the crucial catalytic motifs of the cytosine methyltransferases and is enzymatically inactive *per se* (11). Like Dnmt3a and Dnmt3b, it is highly expressed in ES cells, early embryos and the developing germ cells which undergo dramatic reprogramming of DNA methylation (12–14). Although inactive as an enzyme, knockout experiments have revealed that Dnmt3L is essential for the establishment of maternal methylation imprints during oogenesis, and for the methylation of retrotransposons, satellites repeats and some imprinted genes during spermatogenesis (12,15–19). Biochemical studies demonstrated that Dnmt3L can greatly stimulate the methylation activity of both Dnmt3a and Dnmt3b (20–23). Impaired interaction between DNMT3B and DNMT3L might contribute to the ICF syndrome (14).

Given the role of Dnmt3L in the regulation of the methyltransferase activity, investigation of the regulation of Dnmt3L itself is of potential importance for the understanding of the mechanism of DNA methylation in development and disease. The promoter of *Dnmt3L* has been reported to be unmethylated in ES cells but methylated in somatic tissues, and *in vitro* methylation of *Dnmt3L* with a bacterial methyltransferase inactivated its expression in transfected mammalian cells (24). Despite the inverse correlation of promoter methylation and expression, the mechanistic aspects of *Dnmt3L* methylation and functional significance in development have not been addressed. In this study, we explore these points by genetic and biochemical studies using knockout ES cells and mouse embryos deficient in Dnmt3a, Dnmt3b and Dnmt3L. We show that Dnmt3b is the major methyltransferase responsible for the methylation of the *Dnmt3L* promoter. Dnmt3a and Dnmt3L itself also participate in the methylation process. Hypomethylation due to deficiency in methyltransferase activity causes up-regulation of *Dnmt3L* during the differentiation of mouse ES cells and embryonic development. We therefore conclude that the methylation activity in embryonic cells might be subjected to autorepression at the *Dnmt3L* promoter by the Dnmt3 proteins. Since methylation of the *Dnmt3L* promoter is also impaired in the mouse models for the human ICF syndrome, the deregulation of *DNMT3L* expression could be implicated in the ICF syndrome.

RESULTS

Down-regulation of Dnmt3L in the epiblast and up-regulation in the ExE lineages during the early post-implantation mouse embryonic development

The mouse embryo development of early post-implantation period is characterized by epigenetic reprogramming of cellular fates. Although DNA methyltransferases Dnmt3a and Dnmt3b have been shown to be required for genome-wide *de novo* methylation at the early post-implantation stage (6), mechanistic study of the reprogramming of genomic methylation patterns during this stage is still lacking. To obtain clues about the *de novo* DNA methylation, we prepared specific anti-Dnmt3 antibodies with their performance validated using different knockout ES cells as negative controls (Fig. S1) and examined the expression patterns of Dnmt3a, Dnmt3b and Dnmt3L in the embryonic day (E) 5.5–E7.5 embryos by indirect fluorescence immunostaining. Dnmt3a is found in the epiblast (E5.5–E6.5) and ectoderm (E7.5), and in the visceral and parietal endoderm and trophoblast giant cells (Fig. 1A, E and I). Dnmt3b exists at a high level in the epiblast (E5.5–E6.5) and ectoderm (E7.5), and at a lower but substantial level in the extraembryonic epiblasts (ExEs), the visceral endoderm and the E7.5 mesoderm cells (Fig. 1C, G and K). Interestingly, the expression of Dnmt3L undergoes an obvious transition from the epiblast to ExE over this period. The signal intensity of Dnmt3L decreased gradually in the epiblast, whereas increased in the ExE lineages from E5.5 to E7.5 (Fig. 1B, F and J).

The staining patterns of Dnmt3 proteins at E7.5 match very well with previous reports (6,18). By a more detailed study to distinguish the two Dnmt3a isoforms, we demonstrated that Dnmt3a2 is the predominant form of Dnmt3a in the epiblast (E5.5 and E6.5) and ectoderm (E7.5) (Fig. S2).

Promoter methylation of *Dnmt3L* during early post-implantation development

The temporally and spatially regulated distribution of Dnmt3L in the course of post-implantation development suggests that it may play a role in the control of methylation activity and its expression is subjected to strict control in embryonic development. We next asked whether the promoter of *Dnmt3L* acquires DNA methylation when its expression undergoes repression during this period. To address this question, genomic DNA from epiblasts and ExEs of E5.5, E6.5 and E7.5 embryos was isolated for bisulfite-based methylation analyses. The overall methylation levels were examined by combined bisulfite treatment and restriction analysis

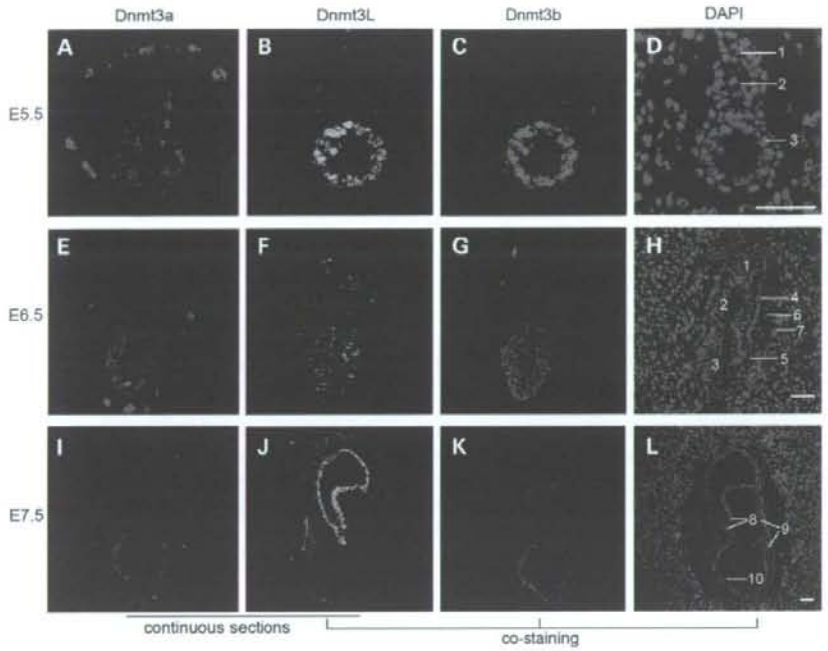

Figure 1. Expression of Dnmt3a, Dnm3b and Dnmt3L in the early post-implantation mouse embryo. Serial sections of mouse embryos at E5.5, E6.5 and E7.5 were immunostained with anti-Dnmt3a full-length (**A, E** and **I**; red), and co-immunostained with monoclonal anti-Dnmt3L (**B, F** and **J**; green) and anti-Dnmt3b full-length (**C, J** and **K**; red) antibodies. Sections were counterstained with the DNA dye DAPI (**D, H** and **L**; blue). 1, ectoplacental cone; 2, extraembryonic epiblast; 3, epiblast; 4, extraembryonic visceral endoderm; 5, embryonic visceral endoderm; 6, parietal endoderm cells; 7, trophoblast giant cells; 8, amniotic folds; 9, extraembryonic and intraembryonic mesoderm; 10, embryonic ectoderm. Scale bar, 50 mm.

(COBRA) on the PCR products derived from bisulfite-treated genomic DNA, and the methylation status of CpG dinucleotides on individual strands was examined by sequencing of clones of the PCR products. The *Dnmt3L* promoter region analyzed contains 16 CpG dinucleotides, and 3 of them are located in the perspective *Taq*I restriction site CCGA (Fig. 2A). The CCGA sequence will be converted to TTGA in the bisulfite-based assay if the second C is unmethylated, but will become TCGA (*Taq*I site) if the second C is methylated. Thus, the cleavage of the PCR products by *Taq*I digestion indicates the presence of a methylated C**C**G**A** site and resistance to *Taq*I digestion reveals the absence of methylation. *Taq*I-based COBRA showed that the *Dnmt3L* promoter is free of methylation at the three analyzed CpG sites in the epiblast at E5.5, but becomes gradually methylated at E6.5 and E7.5 (Fig. 2B). In the ExE, only a small fraction of DNA strands became methylated at E7.5 (Fig. 2B). These observations were confirmed and extended by bisulfite sequencing analysis (Fig. 2C). The overall methylation level rose from 1.8% at E5.5 to 75% at E7.5 in the epiblast. In the ExE, however, methylation was scarce at all time points. The gradual increase in the methylation of *Dnmt3L* promoter in the epiblast coincides well with the gradual decrease in Dnmt3L protein in the early gastrulation stage, whereas the largely unmethylated state in the ExE is conductive to the up-regulation of Dnmt3L in the extraembryonic lineages (Fig. 1B, F and J).

Role of the Dnmt3 members in the promoter methylation and transcriptional repression of *Dnmt3L* during *in vitro* differentiation of ES cells

We then wanted to investigate the enzymes responsible for the methylation of the *Dnmt3L* promoter and the role of DNA methylation in its transcriptional regulation. We employed an *in vitro* stem cell differentiation system which mimics the mouse early embryonic development. The molecular events of cell differentiation in an embryoid body, an induced aggregate of stem cells cultured *in vitro*, are thought to recapitulate early embryonic development to a certain extent (25,26). We first demonstrated that the promoter of *Dnmt3L* is subject to cytosine methylation upon *in vitro* differentiation (Fig. 3A and B). To determine the contribution of Dnmt3a, Dnmt3b and Dnmt3L in the regulation of the *Dnmt3L* promoter, wild-type (WT) and Dnmt3-deficient ES cells were induced to form embryoid bodies (EBs) for differentiation. EBs were collected at different days and subjected to DNA and RNA extraction. Both COBRA and bisulfite sequencing analysis were performed to examine the *Dnmt3L* promoter methylation. As shown in Fig. 3A and B, the *Dnmt3L* promoter underwent gradual methylation in the WT, *Dnmt3a*$^{-/-}$ and *Dnmt3b*$^{-/-}$ ES cells upon differentiation, whereas in the *Dnmt3a*$^{-/-}$/*3b*$^{-/-}$ cells, no methylation was detected. Therefore, both Dnmt3a and Dnmt3b participate in the methylation of the *Dnmt3L* promoter. Interestingly, Dnmt3b has a much larger contribution as the promoter

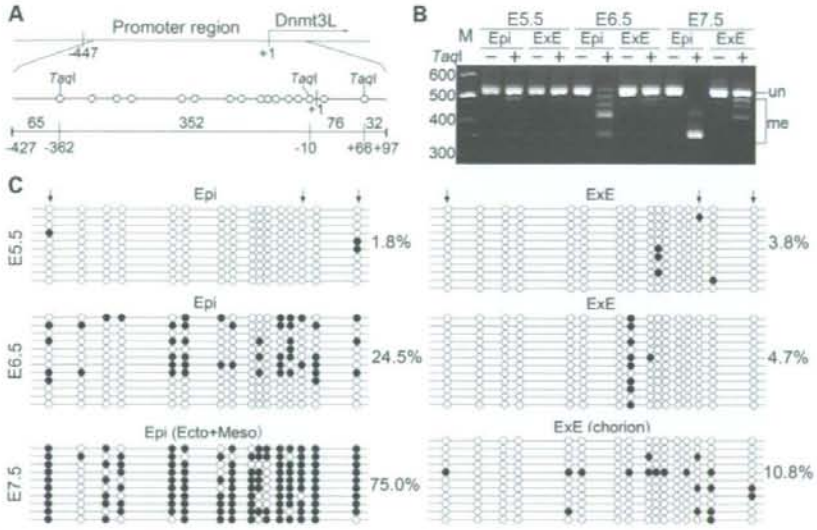

Figure 2. Analysis of DNA methylation of the *Dnmt3L* promoter in the Epi and ExE of early post-implantation mouse embryos. (**A**) Schematic diagram of the *Dnmt3L* promoter (24). The translational starting site is indicated as +1. The relative position of the CpG dinucleotides (open circles) and the *Taq*I sites in the region PCR-amplified after bisulfite treatment are shown below. The lengths of the *Taq*I restriction fragments of the PCR fragment are indicated above the bottom line. (**B**) COBRA methylation analysis of the *Dnmt3L* promoter. For each sample, genomic DNA was obtained from 5–16 embryos. The top band of 524 bp (un) is *Taq*I resistant and the fragments were thus derived from embryonic DNA unmethylated at the CpG dinucleotides within the three *Taq*I sites. The smaller *Taq*I-digested fragments (me) were derived from DNA with full or partial methylation at the analyzed CpG dinucleotides. (**C**) Methylation analysis by bisulfite sequencing. Each line corresponds to a single strand of DNA, and each circle represents an individual CpG dinucleotide. Open circles, unmethylated CpG sties; filled circles, methylated CpG sites. Arrows indicate the CpG dinucleotides within the *Taq*I recognition sequence. Epi, epiblast; ExE, extraembryonic epiblast; Ecto, ectoderm; Meso, mesoderm.

methylation was more severely affected in Dnmt3b-deficient ES cells (Fig. 3A and B). The effect of Dnmt3a deficiency on the methylation rate appeared minimal. Another interesting observation is that Dnmt3L contributes to the methylation of its own promoter. In the absence of Dnmt3L, its promoter methylation was impaired, reaching only 29.4% at day 2 and 48.8% at day 4, significantly lower than the level of WT ES cells at the corresponding time points (Fig. 3A and B). The impairment was not caused by targeted deletion of exons 3–8 of *Dnmt3L* (18), as the promoter region could be methylated by ectopic expression of Dnmt3L in *Dnmt3L*$^{-/-}$ ES cells (Fig. S3).

To analyze the relationship between the altered *Dnmt3L* promoter methylation and expression, we performed real-time RT–PCR to measure the mRNA level at various stages. *Dnmt3L* was first up-regulated upon aggregation (day 1), and then took a down turn in the following days of differentiation in all four ES cell lines (Fig. 3C). Although the overall patterns of change in the mRNA level are similar among different cell lines, the levels of *Dnmt3L* mRNA vary greatly with their genotypes, especially after day 3 when significant promoter methylation of *Dnmt3L* was underway in the WT ES cells. While repression of *Dnmt3L* occurred efficiently in WT ES cells, a significant level of expression persisted in both *Dnmt3b*$^{-/-}$ and double knockout ES cells. In contrast, *Dnmt3L* was efficiently repressed in *Dnmt3a*$^{-/-}$ cells with only a minor elevation of expression at later time points compared with WT ES cells (Fig. 3C). Therefore, comparison of different cell lines indicates that the transcription of *Dnmt3L* during EB differentiation is inversely related to its promoter methylation levels. The high degree of negative correlation strongly suggests that silencing of *Dnmt3L* transcription is closely associated with the occurrence of DNA methylation. On the other hand, the overall down-regulation of *Dnmt3L* transcription regardless of DNA methylation may be accounted for by the contribution of other epigenetic modifications such as histone methylation and/or decrease of transcriptional factors during ES cell differentiation.

Role of the Dnmt3 members in the promoter methylation and transcriptional repression of *Dnmt3L* in embryonic development

To extend our study in the *in vitro* ES cell differentiation system, we next investigated promoter methylation and transcriptional regulation of *Dnmt3L* in mouse embryos. Both the COBRA and bisulfite sequencing were performed on genomic DNA isolated from E9.5 WT and mutant mouse embryos deficient in Dnmt3 proteins (Fig. 4A and B). We found that the *Dnmt3L* promoter was methylated to a similar level of ~58% in the WT and *Dnmt3a*$^{-/-}$ embryos, but the methylation level reached only 12.5 and 42.2% in the absence of *Dnmt3b* or *Dnmt3L*. Removal of both *Dnmt3a* and *Dnmt3b* abolished methylation completely. Defective promoter methylation also led to de-regulation of *Dnmt3L* expression in the mutant embryos (Fig. 4C). Compared with the WT embryos, the *Dnmt3L* mRNA level in the *Dnmt3a*$^{-/-}$, *Dnmt3b*$^{-/-}$ and *Dnmt3a*$^{-/-}$/*3b*$^{-/-}$ embryos was 1.5, 4.2 and 26.5-fold higher, respectively (Fig. 4C, upper panel). In contrast, high level expression of *Dnmt3L* in trophoblast tissues was detected in all samples,

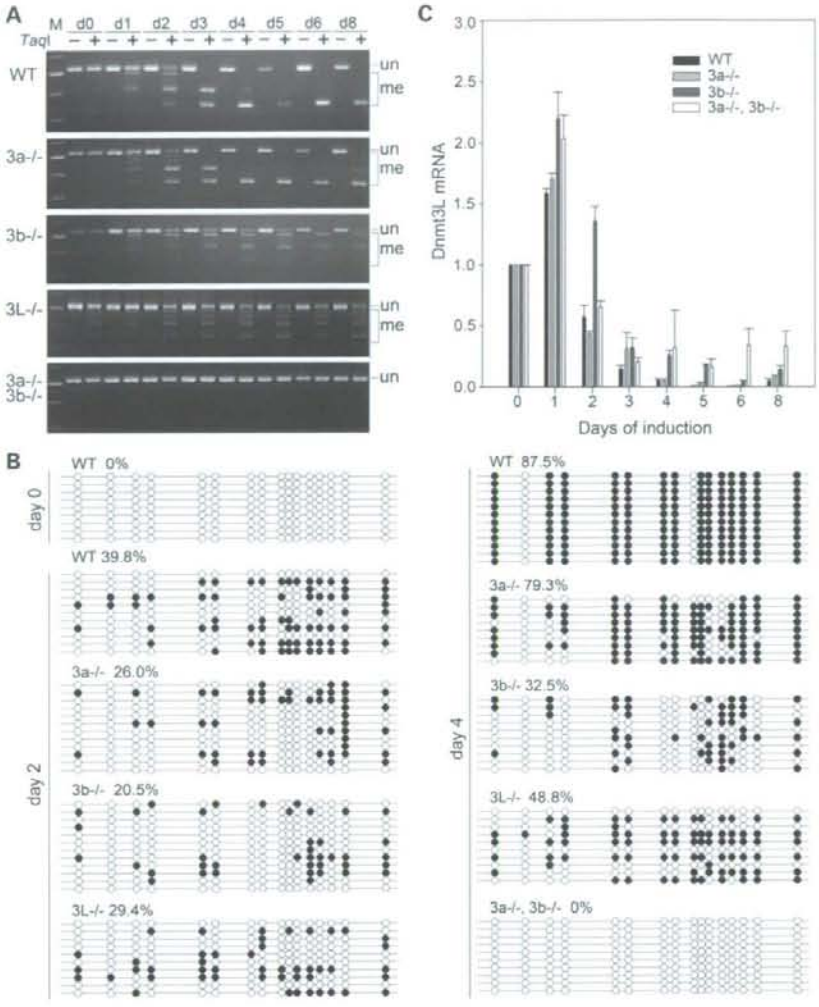

Figure 3. Promoter hypomethylation and increased mRNA levels of *Dnmt3L* in mutant ES cells during *in vitro* differentiation. (**A**) COBRA methylation analysis of the *Dnmt3L* promoter at different stages of differentiation of ES cells. The genotypes of the ES cells (wild-type or Dnmt3 knockout mutant) are indicated at the left and the time points (day 0–8) for methylation analysis indicated on the top. Labeling of the *TaqI* restriction fragment is the same as in Fig. 2B. (**B**) Methylation analysis by bisulfite sequencing. The genotypes of the ES cells (wild-type or Dnmt3 knockout mutant) and the methylation level determined are indicated on the top. The time points (days 0, 2 and 4) for methylation analysis are indicated at the left. (**C**) Analysis of *Dnmt3L* mRNA levels by real-time RT-PCR. The bars represent means ± SD which were derived from three independent experiments each performed in triplicate. The values are relative to the expression level in undifferentiated ES cells (day 0) which was set to 1.

regardless of their genotypes (Fig. 4C, lower panel). These results indicate that all three components of the *de novo* methyltransferases are involved in the promoter methylation of *Dnmt3L* and its transcriptional repression during embryonic development, and Dnmt3b has a predominant contribution.

Hypomethylation of the *Dnmt3L* promoter in mouse ICF models

Deficiency in *DNMT3B* in human ICF patients cause hypomethylation on a number of target sequences including the classic satellite 2 repeats (27). Based on our findings, *DNMT3B* mutations might also affect the methylation of the *DNMT3L* promoter. To address this possibility, we analyzed the methylation status of *Dnmt3L* in mouse ICF models which recapitulate clinical phenotypes (28). Methylation analysis showed that in both brain and tail of ICF mice carrying missense mutations A609T (T/T) and D823G (G/G) in the catalytic domain of Dnmt3b (Fig. 5A), the methylation level of the *Dnmt3L* promoter was severely decreased compared with that of the WT mice (Fig. 5B and C). Quantification by bisulfite sequencing revealed that in the brain of mutant

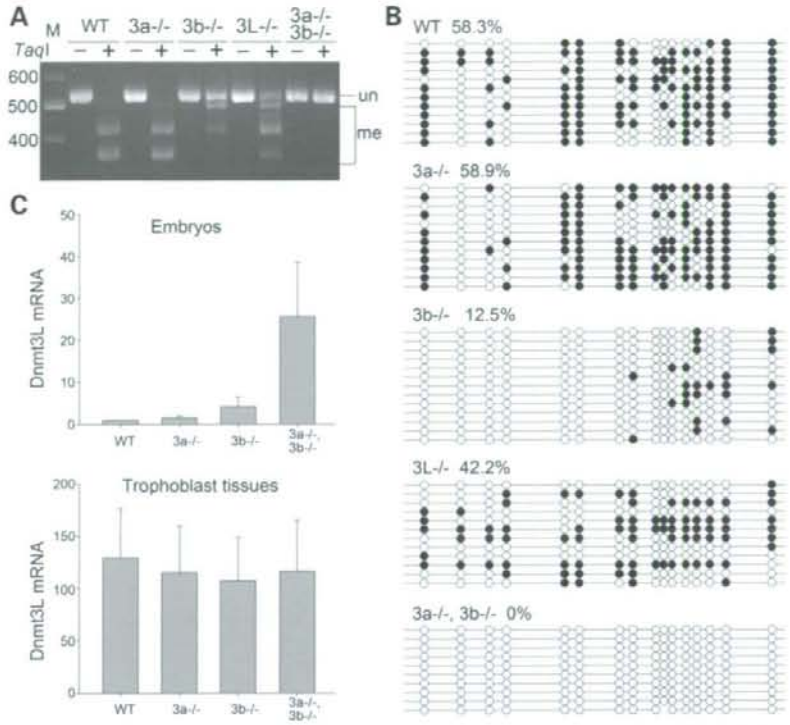

Figure 4. Promoter hypomethylation and increased mRNA levels of *Dnmt3L* in E9.5 mutant mouse embryos. (**A**) COBRA methylation analysis of the *Dnmt3L* promoter. The genotypes of the embryos are indicated on the top. Each DNA sample was obtained from two E9.5 embryos. (**B**) Bisulfite sequencing analysis. (**C**) Analysis of *Dnmt3L* mRNA by real-time RT–PCR. RNA samples of both embryonic and trophoblast tissues were isolated from wild-type ($n = 6$), Dnmt3a$^{-/-}$ ($n = 8$), Dnmt3b$^{-/-}$ ($n = 10$) and Dnmt3a$^{-/-}$/3b$^{-/-}$ ($n = 6$) embryos. The *Dnmt3L* mRNA levels were normalized against the amount of β-actin mRNA in each sample. The bars represent the means ± SD and results are shown as fold up-regulation relative to the level in the wild-type, which was set to 1.

mice, the promoter was only methylated to 34.7 and 50.0%, much lower than 73.6% in the WT. These results further ascertain the critical role of Dnmt3b in the methylation of the *Dnmt3L* promoter during mouse development, and suggest that the functional deficiency of Dnmt3b can not be fully compensated by Dnmt3a and Dnmt3L.

To examine the importance of DNMT3B in the regulation of *DNMT3L* in humans, we first mapped the human *DNMT3L* promoter (Fig. S4). A 250-bp promoter region was confirmed to be methylated upon differentiation of human ES cells *in vitro* (Fig. S5). The region was then analyzed by bisulfite sequencing in the DNA samples from three ICF patients. We found that the methylation levels of the *DNMT3L* promoter in patient leukocytes were modestly lower than in normal controls (Fig. S6).

Recruitment of Dnmt3b to the *Dnmt3L* promoter during ES cell differentiation

Having demonstrated the functional importance of Dnmt3b in the methylation of the *Dnmt3L* promoter in development, we next asked whether Dnmt3b becomes physically associated with the promoter in ES cells upon differentiation. Chromatin immunoprecipitation (ChIP) assay was thus performed in both proliferating (day 0) and differentiating ES cells (day 3). The *Dnmt3b*$^{-/-}$ ES cells aggregate and develop normally during EB differentiation and were used as a negative control in this experiment. Quantification of ChIP data revealed an 11-fold enrichment of Dnmt3b at the *Dnmt3L* promoter upon differentiation of WT ES cells, whereas no significant difference was detected in the *Dnmt3b*$^{-/-}$ ES cells (Fig. 6A). The specificity of the Dnmt3b antibody was validated because control ChIP with the equal amount of mouse IgG showed the background binding in all four samples.

DISCUSSION

During mammalian embryo development, DNA methylation undergoes dramatic reprogramming. Genome-wide demethylation occurs actively on the paternal genome shortly after fertilization and passively on the maternal genome through the subsequent cleavage divisions. Then a wave of *de novo* methylation begins in the inner cell mass probably from the late morula stage, and a considerable level of methylation might become re-established in the blastocyst (29–33). The reprogramming of genomic methylation patterns allows for the establishment of differential gene expression profiles required for lineage specification. For example, early embryonic genes

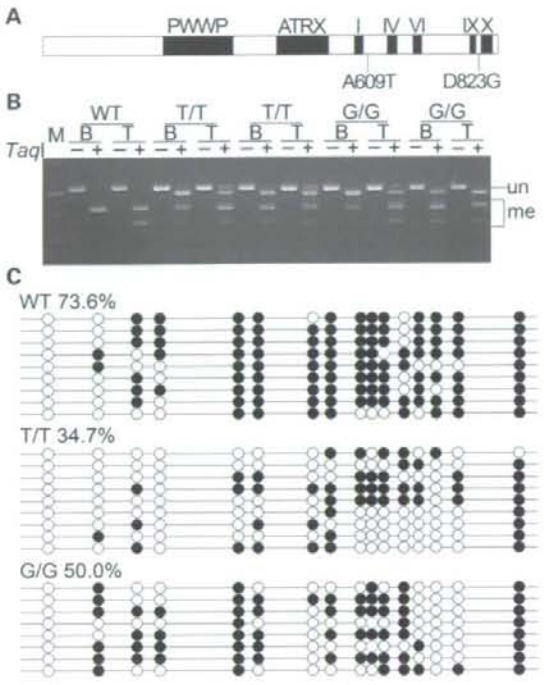

Figure 5. Hypomethylation of the *Dnmt3L* promoter in mouse ICF models. (**A**) Schematic diagram of the mouse Dnmt3b protein. The conserved PWWP and ATRX domains, the conserved motifs (I, IV, VI, IX and X) in the catalytic domain are indicated above. The two ICF mutations made into the mouse models (28) are indicated below. (**B**) COBRA methylation assay of the *Dnmt3L* promoter. Genomic DNA of brains (B) and tails (T) from one wild-type and two mutant mice for each ICF mutation was analyzed. T/T and G/G, the genotypes indicated on the top, represent homozygous A609T and D823G mutations. The DNA samples used were previously described (28). (**C**) Methylation profiles of the *Dnmt3L* promoter revealed by bisulfite sequencing analysis in brain samples. Each DNA sample was obtained from three embryos.

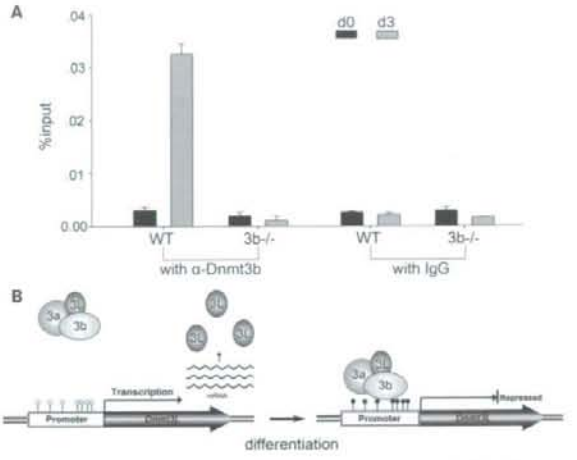

Figure 6. Recruitment of Dnmt3b to the *Dnmt3L* promoter in ES cells upon differentiation. (**A**) Chromatin immunoprecipitation assay in wild-type and *Dnmt3b*$^{-/-}$ ES cells before (day 0) and during (day 3) differentiation. The amount of DNA in immunoprecipitated chromatin was measured by real-time PCR using primers specific for the *Dnmt3L* promoter region. The percentage of signal intensity in immunoprecipitated sample over the input DNA is represented with the bar height. The bars represent means ± SD which were derived from three individual ChIP experiments. (**B**) Model of methylation-mediated auto-suppression of *Dnmt3L* expression. Mechanism controlling the access of Dnmt3 proteins to the promoter is unknown.

such as the pluripotency genes *Oct4* and *Nanog* undergo transcriptional silencing in differentiating cells (34). In the present study, we showed that *Dnmt3L*, a gene controlling DNA methylation, is subjected to epigenetic regulation too. Remarkably, *Dnmt3L* is highly expressed in the early epiblast, and then down-regulated in the embryo proper from mid-gastrulation onwards. The silencing process of *Dnmt3L* is closely correlated with and to a certain extent depends on *de novo* methylation of its promoter. DNA methylation at *Dnmt3L* starts at the onset of gastrulation in the epiblast (E6.5) and reaches a high level by mid-gastrulation (E7.5), a stage when the Dnmt3L protein is missing. All three known components (Dnmt3a, Dnmt3b and Dnmt3L) of the methylation machinery are involved in the process. Deficiency of either component compromises (but does not fully abolish) the methylation activity, resulting in incomplete silencing of *Dnmt3L* in the embryonic cells. Taken together, Dnmt3L, a regulator of *de novo* DNA methylation, is regulated at the transcriptional level by DNA methylation during the early post-implantation period. The mechanistic aspects and biological significance of methylation-mediated *Dnmt3L* silencing are discussed in more detail below.

Contribution of Dnmt3a, Dnmt3b and Dnmt3l in the transcriptional regulation of *Dnmt3L*

We have evaluated the contribution of Dnmt3 proteins in the DNA methylation and transcriptional regulation of *Dnmt3L* in differentiating mutant mouse ES cells *in vitro* and in post-implantation embryos null for *Dnmt3a*, *3b* and *3L*. We found that all the three Dnmt3 members participate in the methylation of the *Dnmt3L* promoter in both the ES cells and embryos. Great variations in the methylation and transcription levels of Dnmt3L were detected among the different single and double knockouts. This has allowed us to assess the contribution of each individual gene in the epigenetic regulation of *Dnmt3L*. We found that Dnmt3b and Dnmt3L have a much larger contribution than Dnmt3a. The level of promoter methylation levels show a nice correlation to the degree of transcriptional silencing in different knockout ES cells and embryos. The sensitive response of transcription to the change of DNA methylation implies that other epigenetic modifications such as histone methylation alone cannot replace the regulatory function of DNA methylation. A seemingly contradictory exception is found with the Dnmt3a-deficient cells and embryos. While having a marginal effect on the establishment of promoter methylation, disruption of *Dnmt3a* causes, respectively, 2.5 (day 5) and 1.5-fold up-regulation of *Dnmt3L* in the differentiating mutant ES cells and the E9.5 knockout embryos (Figs 3C and 4C). Therefore, Dnmt3a has a potential role in transcriptional repression of *Dnmt3L*, independent of its methylation function. This idea fits well with the previous observation that Dnmt3 members are able to mediate transcriptional repression through their

N-terminal PHD domains, which recruit histone deacetylase activities (35–37). Since all Dnmt3 members are present in the early post-implantation embryo (Fig. 1) and they form complexes by direct interaction in embryonic cells (34,38), we postulate that Dnmt3a might cooperate with Dnmt3b and Dnmt3L mainly as a transcription repressor at the *Dnmt3L* locus during development. This may account for a strong synergistic effect between the two methyltransferases, mostly obviously seen in experiments with knockout embryos: the up-regulation of *Dnmt3L* in the double knockout E9.5 embryos exceeds by 4.6-fold over the sum of that in the *Dnmt3a* and *Dnmt3b* single knockout embryo (Fig. 4C). The cooperation in the transcriptional repression of *Dnmt3L* in a methylation-independent fashion appears to be different from the situation of the epigenetic regulation of the *Oct4* and *Nanog* genes we reported previously (34). Dnmt3a and Dnmt3b show a clear synergistic effect both in the methylation of the *Oct4* and *Nanog* promoters and in their transcriptional silencing. Another previous report showed that *Dnmt3a* and *Dnmt3b* are required to maintain the methylation at a regulatory region of the oocyte-specific form of the *Dnmt1* gene in ES cells (7). It remains unresolved whether the maintenance methylation at the *Dnmt3L*, *Oct4* and *Nanog* promoters upon cell differentiation would also involve the two Dnmt3 enzymes.

Auto-repression of the methyltransferase activity by the promoter methylation of *Dnmt3L*

Though Dnmt3L lacks intrinsic methyltransferase activity, it is well established that it serves as a key regulator of DNA methylation. Besides its function in stimulating the activity of both Dnmt3a and Dnmt3b (20–22), more recent biochemical studies have shown that Dnmt3L has a potential targeting function in the determination of specific genomic loci to be methylated. Complex of Dnmt3L with Dnmt3a C-terminal domains might contribute to the recognition of the differentially methylated region of maternal imprinted genes (39). Dnmt3L can also bind via its N-terminal PHD domain specifically to unmethylated lysine 4 of H3, potentially mediating the recruitment of Dnmt3a enzymes to inactive chromatin regions (38). The dual ability of Dnmt3L in enzymatic stimulation and target-specific recruitment of Dnmt3a and 3b makes its expression a good regulatory point. Interestingly, different promoters have been reported to control the expression of sex-specific *Dnmt3L* isoforms in mouse germ cells (40).

Based on the regulatory function of the Dnmt3 members in the expression of *Dnmt3L* in mouse ES cells and embryos, we postulate an auto-repression mechanism for the control of the cellular methylation activity (Fig. 6B). If the *de novo* methyltransferase activity is excessive, the methylation machinery might feed back negatively to the Dnmt3L activator by promoter methylation. Conversely, if the methyltransferase activity is too low, for example, due to a point mutation in a methyltransferase, the negative feed-back system may allow overexpression or delayed silencing of *Dnmt3L*, thus resulting in a compensation of the methylation activity. The self-adjustment of the total methyltransferase activity might help establish precise genomic methylation patterns in development. This model does not exclude the importance of other epigenetic mechanisms in the transcriptional regulation of *Dnmt3L*. The high expression level of all Dnmt3 members in ES and epiblast cells indicates that unknown factor(s) protecting the *Dnmt3L* promoter from methylation and silencing remain yet to be identified.

The developmental significance of the regulation of Dnmt3L

At the commencement of gastrulation, most target sequences in the genome has been methylated in the wave of the genome-wide methylation beginning from the late morula (29,30,33). The subsequent development of embryo involves rapid cellular migration and differentiation by which the progenitors of different cell lineages are produced. This process might involve the methylation or demethylation of tissue-specific genes to generate various lineages. The dynamic expression of Dnmt3L in the early embryo may suggest a role of Dnmt3L in the *de novo* methylation of the genome. This view is apparently at odd with a lack of any somatic phenotype in the *Dnmt3L* knockout mice (15,18). However, the *Dnmt3L* knockout mice which were phenotypically normal were invariably derived from a heterozygous mother and a heterozygous father. The heterozygous mother could have deposited Dnmt3L in the oocytes and this deposit could support the early development of the homozygous embryo. Indeed, *Dnmt3L* is actively transcribed in the growing oocyte (18). Therefore, the characterization of a Dnmt3L embryonic function requires a careful phenotype analysis and genome-wide methylation profiling in the mutant embryos obtained with a new cross (*Dnmt3L* homozygous mother × *Dnmt3L* heterozygous father).

Dnmt3L, as a general activator of *de novo* methyltransferases, might have to be down-regulated after the early genome-wide *de novo* methylation has completed. If the expression of *Dnmt3L* would persist, further differentiation of the epiblast and germ layers might be disturbed due to excessive methylation. In fact, in our study of the *Dnmt3L* transgenic mice, we found that the expression of an extremely low level of *Dnmt3L* might be incompatible with normal development (unpublished data). Excessive methylation activity in the case of forced expression of transgenic Dnmt3b in post-natal mouse led to abnormal methylation and neoplasia (41). A recent survey for cervix cancer suggests that up-regulation of *DNMT3L* due to promoter hypomethylation might contribute to tumorigenesis in human (42).

The ICF syndrome is the only human genetic disease known to arise from germline mutations within a DNA methyltransferase gene—*DNMT3B*. Like most other *DNMT3B* mutations, the two mutations (A609T and D823G) used in the mouse models affect the catalytic domain and thus attenuate the enzymatic activity (27,28). Both mutant proteins also display an altered nuclear subcellular localization, with less accumulation at the pericentric heterochromatin (28). Since the *Dnmt3L* promoter is hypomethylated in the mouse models of the human ICF syndrome, we speculate that dysregulation of *DNMT3L* might also occur during ICF fetal development and thus influence the phenotype formation. A modest decrease in the methylation of a *DNMT3L* promoter region was indeed detected in the leukocytes from three ICF patients (Fig. S6).

The less-severe hypomethylation in the human ICF might be explained by the following aspects. First, the human ICF samples used were leukocytes, while tail and brain DNA were analyzed for the mouse model. Second, ICF probands show great phenotypic variation. ICF mothers have a lot of spontaneous abortion. The born ICF fetuses and long-surviving patients have less-severe phenotypes in general. The patients we analyzed were born and are probably the ones that were 'more' viable. Therefore, samples from aborted ICF fetuses would be more appropriate for examining hypomethylation at the *DNMT3L* promoter.

Up-regulation of DNMT3L due to hypomethylation during embryonic development could partially compensate the deficiency in methylation activity caused by *DNMT3B* mutations, ensuring proper methylation at most genomic loci. This would mitigate the adverse effect of the DNMT3B deficiency. This idea is consistent with the finding that hypomethylation in ICF patients is restricted to a small portion of the genome (27,43). On the other hand, over-activation of DNMT3A or 3B by the up-regulated DNMT3L could lead to abnormal methylation of otherwise unmethylated sequences as most ICF mutant proteins retain a considerable amount of catalytic activity (14). Assessment of this possibility would require thorough genome-wide methylation profiling of ICF cells.

MATERIALS AND METHODS

Antibodies and immunofluorescence

The polyclonal anti-Dnmt3a (full-length) and anti-Dnmt3b (full-length) antibodies and monoclonal anti-Dnmt3L have been described previously (14,44). Immunostaining of embryo cross-sections was performed as previously described (12), and the images were captured with a confocal microscope (Leica TCS SP2 AOBS).

Mice and embryos

CD-1 mice were purchased from the Shanghai Laboratory Animal Center (Chinese Academy of Sciences). Dnmt3 knockout mice were described previously (6,18). Mice of ICF models were described previously (28). Noon of the day on which the vaginal plug was seen was designated as E0.5. The mouse epiblasts and ExEss were isolated under a Nikon SMZ-1500 stereomicroscope, washed three times in M2 medium, and stored at −70°C until use.

Bisulfite methylation analysis

Bisulfite treatment of genomic DNA was carried out as previously described (45). Nested PCR was performed to amplify the *Dnmt3L* promoter region with the following primers: outside forward, ATT TTA ATG TGT GAG GTT TAG AGT TTT T; outside reverse, ACC TAA AAA TCT CAC AAA ATT TCA AC; inside forward, GTT TTG AGT TTT ATA GAA TTT TAT AAT TTT T; inside reverse, AAA AAC TAT CAA CAT CAA AAC TAA AAC. The annealing temperature was 57°C (with 1.5 mM Mg^{2+}) for the first round of PCR and 59°C (with 3 mM Mg^{2+}) for the second round. For COBRA analysis, 5 μl of the PCR products were restricted with *Taq*I (Takara) followed by electrophoresis in 3% agarose gel. For sequencing analysis, the PCR products were cloned into T-vectors (Takara Inc.), and individual clones were sequenced by Invitrogen Ltd, Shanghai.

ES cell culture and *in vitro* differentiation

WT and mutant ES cells were maintained as preciously described (46). To induce differentiation, ES cells were cultured for two days by the hanging drop method (700 ES cells per 20 μl in each drop) (47). EBs in hanging drops were then transferred to 100 mm Petri dishes and cultured in suspension for various days.

Quantitative RT–PCR

Total RNA was isolated from ES cells or tissues with TRIzol (Invitrogen) according to the manufacturer's instructions. Reverse-transcription was performed using the reverse transcription system (Promega Ltd) with oligonucleotide dT primer. The quantification of transcripts was performed by real-time PCR on a Realplex 2S cycler (Eppendorf Ltd) using Eva Green fluorescent dye (Biotium Inc.) according to the standard curve method (48). Expression values were normalized to that of β-actin. The PCR primers for *Dnmt3L* were as described (13) and the mouse β-actin primers were as follows: forward, TTC CTT CTT GGG TAT GGA AT; reverse, GAG CAA TGA TCT TGA TCT TC. Annealing temperatures for both reactions were 60°C.

Chromatin immunoprecipitation

The ChIP assay was carried out largely as described (49). Briefly, trypsin dispersed cells were treated with 1.42% formaldehyde for 15 min at room temperature, followed by incubation with a 0.125 M glycine solution for 5 min. Nuclei were then extracted and incubated in nuclear lysis buffer for 20 min. The genomic DNA was sheared to an average size of 500 bp with a Diagenode BioRuptor™ sonicator [16 times for ES cells and 14 times for EB cells (30 s/pulse with 1 min rest interval)]. The sheared extracts were diluted 10-fold by ChIP dilution buffer, precleared with salmon sperm DNA, BSA and protein A/G agarose beads and incubated with 3 μg antibody (monoclonal anti-Dnmt3b or mouse IgG) at 4°C overnight. Blocked protein A/G agarose beads (50 μl, 50% slurry) were then added and rotated at 4°C for 2 h followed by centrifugation. The supernatant from the control precipitation was used as input. The beads were washed and bound DNA was eluted with elution buffer (1% SDS, and 100 mM $NaHCO_3$). The eluates were then de-cross-linked and treated with proteinase K for DNA purification. The immunoprecipitated DNA was analyzed by real-time PCR with primers specific for the *Dnmt3L* promoter (forward, CCT CAT AGG CTC CAT CCA GCA T; reverse, CAG GGT CGT CAG AAC CCT AAA ACG; annealing temperature, 65°C). To process the ChIP data, the percentage of immunoprecipitated DNA over the input was calculated.

SUPPLEMENTARY MATERIAL

Supplementary Material is available at HMG Online.

ACKNOWLEDGEMENTS

We thank Dr F. Tang for critic review of the manuscript.

Conflict of Interest statement. None declared.

FUNDING

This work was supported by grants from the Max- Planck-Gesellschaft of Germany and the Ministry of Science and Technology of China (2005CB522400 and 2007CB947503) and the National Science Foundation of China (30730059) to G.L.X.

REFERENCES

1. Jones, P.A. and Baylin, S.B. (2007) The epigenomics of cancer. *Cell*, **128**, 683–692.
2. Feinberg, A.P. (2007) Phenotypic plasticity and the epigenetics of human disease. *Nature*, **447**, 433–440.
3. Morgan, H.D., Santos, F., Green, K., Dean, W. and Reik, W. (2005) Epigenetic reprogramming in mammals. *Hum. Mol. Genet.*, **14**, R47–R58.
4. Bestor, T.H. (2000) The DNA methyltransferases of mammals. *Hum. Mol. Genet.*, **9**, 2395–2402.
5. Okano, M., Xie, S. and Li, E. (1998) Cloning and characterization of a family of novel mammalian DNA (cytosine-5) methyltransferases. *Nat. Genet.*, **19**, 219–220.
6. Okano, M., Bell, D.W., Haber, D.A. and Li, E. (1999) DNA methyltransferases Dnmt3a and Dnmt3b are essential for de novo methylation and mammalian development. *Cell*, **99**, 247–257.
7. Ko, Y.G., Nishino, K., Hattori, N., Arai, Y., Tanaka, S. and Shiota, K. (2005) Stage-by-stage change in DNA methylation status of Dnmt1 locus during mouse early development. *J. Biol. Chem.*, **280**, 9627–9634.
8. Chen, T., Ueda, Y., Xie, S. and Li, E. (2002) A novel Dnmt3a isoform produced from an alternative promoter localizes to euchromatin and its expression correlates with active de novo methylation. *J. Biol. Chem.*, **277**, 38746–38754.
9. Xu, G.L., Bestor, T.H., Bourc'his, D., Hsieh, C.L., Tommerup, N., Bugge, M., Hulten, M., Qu, X., Russo, J.J. and Viegas-Pequignot, E. (1999) Chromosome instability and immunodeficiency syndrome caused by mutations in a DNA methyltransferase gene. *Nature*, **402**, 187–191.
10. Hansen, R.S., Wijmenga, C., Luo, P., Stanek, A.M., Canfield, T.K., Weemaes, C.M. and Gartler, S.M. (1999) The DNMT3B DNA methyltransferase gene is mutated in the ICF immunodeficiency syndrome. *Proc. Natl Acad. Sci. USA*, **96**, 14412–14417.
11. Aapola, U., Shibuya, K., Scott, H.S., Ollila, J., Vihinen, M., Heino, M., Shintani, A., Kawasaki, K., Minoshima, S., Krohn, K. *et al.* (2000) Isolation and initial characterization of a novel zinc finger gene, DNMT3L, on 21q22.3, related to the cytosine-5-methyltransferase 3 gene family. *Genomics*, **65**, 293–298.
12. Bourc'his, D. and Bestor, T.H. (2004) Meiotic catastrophe and retrotransposon reactivation in male germ cells lacking Dnmt3L. *Nature*, **431**, 96–99.
13. La Salle, S., Mertineit, C., Taketo, T., Moens, P.B., Bestor, T.H. and Trasler, J.M. (2004) Windows for sex-specific methylation marked by DNA methyltransferase expression profiles in mouse germ cells. *Dev. Biol.*, **268**, 403–415.
14. Xie, Z.H., Huang, Y.N., Chen, Z.X., Riggs, A.D., Ding, J.P., Gowher, H., Jeltsch, A., Sasaki, H., Hata, K. and Xu, G.L. (2006) Mutations in DNA methyltransferase DNMT3B in ICF syndrome affect its regulation by DNMT3L. *Hum. Mol. Genet.*, **15**, 1375–1385.
15. Bourc'his, D., Xu, G.L., Lin, C.S., Bollman, B. and Bestor, T.H. (2001) Dnmt3L and the establishment of maternal genomic imprints. *Science*, **294**, 2536–2539.
16. Kato, Y., Kaneda, M., Hata, K., Kumaki, K., Hisano, M., Kohara, Y., Okano, M., Li, E., Nozaki, M. and Sasaki, H. (2007) Role of the Dnmt3 family in de novo methylation of imprinted and repetitive sequences during male germ cell development in the mouse. *Hum. Mol. Genet.*, **16**, 2272–2280.
17. Webster, K.E., O'Bryan, M.K., Fletcher, S., Crewther, P.E., Aapola, U., Craig, J., Harrison, D.K., Aung, H., Phutikanit, N., Lyle, R. *et al.* (2005) Meiotic and epigenetic defects in Dnmt3L-knockout mouse spermatogenesis. *Proc. Natl Acad. Sci. USA*, **102**, 4068–4073.
18. Hata, K., Okano, M., Lei, H. and Li, E. (2002) Dnmt3L cooperates with the Dnmt3 family of de novo DNA methyltransferases to establish maternal imprints in mice. *Development*, **129**, 1983–1993.
19. Hata, K., Kusumi, M., Yokomine, T., Li, E. and Sasaki, H. (2006) Meiotic and epigenetic aberrations in Dnmt3L-deficient male germ cells. *Mol. Reprod. Dev.*, **73**, 116–122.
20. Chedin, F., Lieber, M.R. and Hsieh, C.L. (2002) The DNA methyltransferase-like protein DNMT3L stimulates de novo methylation by Dnmt3a. *Proc. Natl Acad. Sci. USA*, **99**, 16916–16921.
21. Suetake, I., Shinozaki, F., Miyagawa, J., Takeshima, H. and Tajima, S. (2004) DNMT3L stimulates the DNA methylation activity of Dnmt3a and Dnmt3b through a direct interaction. *J. Biol. Chem.*, **279**, 27816–27823.
22. Gowher, H., Liebert, K., Hermann, A., Xu, G. and Jeltsch, A. (2005) Mechanism of stimulation of catalytic activity of Dnmt3A and Dnmt3B DNA-(cytosine-C5)-methyltransferases by Dnmt3L. *J. Biol. Chem.*, **280**, 13341–13348.
23. Chen, Z.X., Mann, J.R., Hsieh, C.L., Riggs, A.D. and Chedin, F. (2005) Physical and functional interactions between the human DNMT3L protein and members of the de novo methyltransferase family. *J. Cell. Biochem.*, **95**, 902–917.
24. Aapola, U., Maenpaa, K., Kaipia, A. and Peterson, P. (2004) Epigenetic modifications affect Dnmt3L expression. *Biochem. J.*, **380**, 705–713.
25. Weitzer, G. (2006) Embryonic stem cell-derived embryoid bodies: an in vitro model of eutherian pregastrulation development and early gastrulation. *Handbook of Experimental Pharmacology*, 21–51.
26. Leahy, A., Xiong, J.W., Kuhnert, F. and Stuhlmann, H. (1999) Use of developmental marker genes to define temporal and spatial patterns of differentiation during embryoid body formation. *J. Exp. Zool.*, **284**, 67–81.
27. Ehrlich, M. (2003) The ICF syndrome, a DNA methyltransferase 3B deficiency and immunodeficiency disease. *Clin. Immunol.*, **109**, 17–28.
28. Ueda, Y., Okano, M., Williams, C., Chen, T., Georgopoulos, K. and Li, E. (2006) Roles for Dnmt3b in mammalian development: a mouse model for the ICF syndrome. *Development*, **133**, 1183–1192.
29. Monk, M., Boubelik, M. and Lehnert, S. (1987) Temporal and regional changes in DNA methylation in the embryonic, extraembryonic and germ cell lineages during mouse embryo development. *Development*, **99**, 371–382.
30. Kafri, T., Ariel, M., Brandeis, M., Shemer, R., Urven, L., McCarrey, J., Cedar, H. and Razin, A. (1992) Developmental pattern of gene-specific DNA methylation in the mouse embryo and germ line. *Genes Dev.*, **6**, 705–714.
31. Mayer, W., Niveleau, A., Walter, J., Fundele, R. and Haaf, T. (2000) Demethylation of the zygotic paternal genome. *Nature*, **403**, 501–502.
32. Oswald, J., Engemann, S., Lane, N., Mayer, W., Olek, A., Fundele, R., Dean, W., Reik, W. and Walter, J. (2000) Active demethylation of the paternal genome in the mouse zygote. *Curr. Biol.*, **10**, 475–478.
33. Santos, F., Hendrich, B., Reik, W. and Dean, W. (2002) Dynamic reprogramming of DNA methylation in the early mouse embryo. *Dev. Biol.*, **241**, 172–182.
34. Li, J.Y., Pu, M.T., Hirasawa, R., Li, B.Z., Huang, Y.N., Zeng, R., Jing, N.H., Chen, T., Li, E., Sasaki, H. *et al.* (2007) Synergistic function of DNA methyltransferases Dnmt3a and Dnmt3b in the methylation of Oct4 and Nanog. *Mol. Cell. Biol.*, **27**, 8748–8759.
35. Fuks, F., Burgers, W.A., Godin, N., Kasai, M. and Kouzarides, T. (2001) Dnmt3a binds deacetylases and is recruited by a sequence-specific repressor to silence transcription. *EMBO J.*, **20**, 2536–2544.
36. Bachman, K.E., Rountree, M.R. and Baylin, S.B. (2001) Dnmt3a and Dnmt3b are transcriptional repressors that exhibit unique localization properties to heterochromatin. *J. Biol. Chem.*, **276**, 32282–32287.

37. Aapola, U., Liiv, I. and Peterson, P. (2002) Imprinting regulator DNMT3L is a transcriptional repressor associated with histone deacetylase activity. *Nucleic Acids Res.*, **30**, 3602–3608.
38. Ooi, S.K., Qiu, C., Bernstein, E., Li, K., Jia, D., Yang, Z., Erdjument-Bromage, H., Tempst, P., Lin, S.P., Allis, C.D. *et al.* (2007) DNMT3L connects unmethylated lysine 4 of histone H3 to de novo methylation of DNA. *Nature*, **448**, 714–717.
39. Jia, D., Jurkowska, R.Z., Zhang, X., Jeltsch, A. and Cheng, X. (2007) Structure of Dnmt3a bound to Dnmt3L suggests a model for de novo DNA methylation. *Nature*, **449**, 248–251.
40. Shovlin, T.C., Bourc'his, D., La Salle, S., O'Doherty, A., Trasler, J.M., Bestor, T.H. and Walsh, C.P. (2007) Sex-specific promoters regulate Dnmt3L expression in mouse germ cells. *Hum. Reprod.*, **22**, 457–467.
41. Linhart, H.G., Lin, H., Yamada, Y., Moran, E., Steine, E.J., Gokhale, S., Lo, G., Cantu, E., Ehrich, M., He, T. *et al.* (2007) Dnmt3b promotes tumorigenesis in vivo by gene-specific de novo methylation and transcriptional silencing. *Genes Dev.*, **21**, 3110–3122.
42. Gokul, G., Gautami, B., Malathi, S., Sowjanya, A.P., Poli, U.R., Jain, M., Ramakrishna, G. and Khosla, S. (2007) DNA methylation profile at the DNMT3L promoter: a potential biomarker for cervical cancer. *Epigenetics*, **2**, 80–85.
43. Shirohzu, H., Kubota, T., Kumazawa, A., Sado, T., Chijiwa, T., Inagaki, K., Suetake, I., Tajima, S., Wakui, K., Miki, Y. *et al.* (2002) Three novel DNMT3B mutations in Japanese patients with ICF syndrome. *Am. J. Med. Genet.*, **112**, 31–37.
44. Ge, Y.Z., Pu, M.T., Gowher, H., Wu, H.P., Ding, J.P., Jeltsch, A. and Xu, G.L. (2004) Chromatin targeting of de novo DNA methyltransferases by the PWWP domain. *J. Biol. Chem.*, **279**, 25447–25454.
45. Hajkova, P., el-Maarri, O., Engemann, S., Oswald, J., Olek, A. and Walter, J. (2002) DNA-methylation analysis by the bisulfite-assisted genomic sequencing method. *Methods Mol. Biol.*, **200**, 143–154.
46. Chen, T., Ueda, Y., Dodge, J.E., Wang, Z. and Li, E. (2003) Establishment and maintenance of genomic methylation patterns in mouse embryonic stem cells by Dnmt3a and Dnmt3b. *Mol. Cell. Biol.*, **23**, 5594–5605.
47. Metzger, J.M., Lin, W.I. and Samuelson, L.C. (1994) Transition in cardiac contractile sensitivity to calcium during the in vitro differentiation of mouse embryonic stem cells. *J. Cell Biol.*, **126**, 701–711.
48. Bustin, S.A. (2002) Quantification of mRNA using real-time reverse transcription PCR (RT-PCR): trends and problems. *J. Mol. Endocrinol.*, **29**, 23–39.
49. Yu, Q., Thieu, V.T. and Kaplan, M.H. (2007) Stat4 limits DNA methyltransferase recruitment and DNA methylation of the IL-18Ralpha gene during Th1 differentiation. *EMBO J.*, **26**, 2052–2060.